
Volume 316, Number 2, December 15, 2007
This Number Completes Volume 316
ISSN 0021-9797
ELSEVIER
JOURNAL OF
Colloid and
Interface Science
EDITOR-IN-CHIEF
Darsh T. Wasan
Illinois Institute of Technology, Chicago
CO-EDITORS
Julian Eastoe University of Bristol, United Kingdom
Arthur T. Hubbard Santa Barbara Science Project, California
Manuel Arturo López-Quintela University of Santiago de Compostela, Spain
Gao Qing Lu University of Queensland, Australia
Martin Malmsten Uppsala University, Sweden
ADVISORY BOARD
Masahiko Abe Chiba, Japan
Pierre M. Adler Paris, France
Jayesh Bellare Mumbai, India
Marcel Böhmer Eindhoven, Netherlands
Peter Bräuer Leipzig, Germany
Richard Finke Colorado, USA
Peter Griffiths Cardiff, UK
Andrew Howe Cambridge, UK
Marek Kosmulski Lublin, Poland
Dongqing Li Tennessee, USA
Louis Liz Marzan Vigo, Spain
Stefano A. Mezzasalma Trieste, Italy
Jerzy Mielczarski Vandoeuvre-les-Nancy, France
Catherine J. Murphy South Carolina, USA
Tommy Nylander Lund, Sweden
Clive A. Prestidge Mawson Lakes, Australia
John Ralston Mawson Lakes, Australia
Eli Ruckenstein New York, USA
Lynn M. Walker Pennsylvania, USA
Gregory G. Warr Sydney, Australia
Fernando Wypych Curitiba, Brazil
Joseph Zazadzinski California, USA
Thomas Zemb Gif-sur-Yvette, France
Dongyuan Zhao Shanghai, China
Victor K. La Mer, Editor 1946–1965
Albert C. Zettlemoyer, Co-Editor 1965–1987
Milton Kerker, Co-Editor 1965–1987, Editor 1987–1992
Josip P. Kratohvil, Co-Editor 1987–2004
Hironobu Kunieda, Co-Editor 2004–2005

Available online at www.sciencedirect.com
ScienceDirect
ELSEVIER
Journal of Colloid and Interface Science 316 (2007) 844–857
Journal of Colloid and Interface Science
www.elsevier.com/locate/jcis

Hydrodynamic forces acting on a microscopic emulsion drop growing at a capillary tip in relation to the process of membrane emulsification

Krassimir D. Danov, Darina K. Danova [1], Peter A. Kralchevsky *

Laboratory of Chemical Physics and Engineering, Faculty of Chemistry, University of Sofia, 1164 Sofia, Bulgaria

Received 4 May 2007; accepted 18 August 2007

Available online 31 August 2007

Abstract

Here, we calculate the hydrodynamic ejection force acting on a microscopic emulsion drop, which is continuously growing at a capillary tip. This force could cause drop detachment in the processes of membrane and microchannel emulsification, and affect the size of the released drops. The micrometer-sized drops are not deformed by gravity and their formation happens at small Reynolds numbers despite the fact that the typical period of drop generation is of the order of 0.1 s. Under such conditions, the flow of the disperse phase through the capillary, as it inflates the droplet, engenders a hydrodynamic force, which has a predominantly viscous (rather than inertial) origin. The hydrodynamic boundary problem is solved numerically, by using appropriate curvilinear coordinates. The spatial distributions of the stream function and the velocity components are computed. The hydrodynamic force acting on the drop is expressed in terms of three universal functions of the ratio of the pore and drop radii. These functions are computed numerically. Interpolation formulas are obtained for their easier calculation. It turns out that the increase in the viscosity of each of the two liquid phases increases the total ejection force. The results could find applications for the interpretation and prediction of the effect of hydrodynamic factors on the drop size in membrane emulsification.

Keywords: Membrane emulsification; Microchannel emulsification; Hydrodynamic forces; Drop formation at capillary tip

1. Introduction

The method of membrane emulsification attracted a considerable interest and found numerous applications during the last decade. The method was applied in many fields, in which monodisperse emulsions are needed. In food industry it was used for production of oil-in-water (O/W) emulsions: dressings, artificial milk, cream liqueurs, as well as for preparation of some water-in-oil (W/O) emulsions: margarine and low-fat spreads. Another application of this method is for fabrication of monodisperse colloidal particles: silica–hydrogel and polymer microspheres; porous and cross-linked polymer particles; microspheres containing carbon black for toners, etc. A third field is the production of multiple emulsions and microcapsules, which have found applications in pharmacy and chemotherapy. Detailed reviews could be found in Refs. [1–5]. Closely related to the membrane emulsification is the method employing capillary tubes or microchannels to produce monodisperse emulsions [6–9].

The key problem of membrane emulsification is related to the explanation and prediction of the dependence of the drop size on the system's parameters: pore diameter; flux of the disperse phase along the pores; applied cross flow in the continuous phase; viscosity of the oil and water phases; interfacial tension and kinetics of surfactant adsorption, etc. (Here and hereafter we call "disperse" the phase from which the drops are made, despite the fact that this phase is continuous before the drop detachment from the membrane.) Different approaches have been used to solve this problem: by regression analysis of experimental data [9]; by modeling of the drop expansion and surfactant adsorption by surface evolver [10,11]; by three-dimensional computational fluid dynamics simulations [12,13], and by lattice Boltzmann simulations [14]. The quantitative the-

* Corresponding author. Fax: +359 2 962 5438.
E-mail address: pk@lcpe.uni-sofia.bg (P.A. Kralchevsky).
[1] Present address: Division of Physics & Astronomy, Vrije Universiteit Amsterdam, 1081HV Amsterdam, The Netherlands.

0021-9797/$ – see front matter © 2007 Elsevier Inc. All rights reserved.
doi:10.1016/j.jcis.2007.08.061

oretical analysis demands one to determine the forces exerted on the growing emulsion drop and to establish the mechanism of drop detachment from the pores.

In some experiments, cross flow is applied in the continuous phase parallel to the membrane surface. It gives rise to *drag* and *lift* hydrodynamic forces that tilt the protruding drop and help for its detachment from the membrane [4,14,15]. In addition, the flow of the disperse phase through the capillary, as it inflates the droplet, engenders a hydrodynamic *ejection* force that also tends to detach the droplet from the pore [15].

It is possible to produce monodisperse emulsions by membrane emulsification in the absence of cross flow in the outer liquid phase [3]. In this case, the drag and lift hydrodynamic forces are missing, but the ejection force alone is able to detach the drops from the pores. The hydrodynamic estimates (see Section 3 below) show that under typical experimental conditions this process happens at small Reynolds numbers, for which the inertial terms in the Navier–Stokes equation are negligible. Hence, under such conditions the ejection force has a predominantly viscous (rather than inertial) character.

The full hydrodynamic problem for detachment of emulsion drops in cross flow is rather complicated. It could be split into two separate problems: (i) calculation of the ejection force in the absence of cross flow in the outer liquid, and (ii) accounting for the effect of the cross flow. Our goal in the present article is to solve the first problem.

The paper is organized as follows. In Section 2, we consider the kinematics of drop expansion. In Section 3, the basic equations and boundary conditions are formulated. In Section 4, appropriate curvilinear coordinates are introduced to transform the three physical domains (capillary channel, drop and outer phase) into rectangles. The hydrodynamic boundary problem is solved numerically and the velocity field is calculated. Finally, in Section 5 the hydrodynamic force acting on the emulsion drop is computed and interpolation formulas are obtained for its easier calculation. Details of the theoretical derivations are given as appendices to this paper—see Supplementary material.

2. Kinematics of drop expansion

We consider the expansion of an emulsion drop, which is growing at the tip of a capillary. Our purpose is to quantify the hydrodynamic forces acting on the drops, which are formed at the openings of the pores of an emulsification membrane. We are dealing with microscopic drops, for which the gravitational deformation of the drop is negligible. Here, we consider the simpler case, in which there is no cross-flow in the outer liquid phase; i.e., the only motion in the outer liquid is due to its displacement by the growing drop.

Because we are dealing with small drops, we will simplify our treatment by the assumption that the drop surface is (approximately) spherical. The membrane pore will be modeled as a cylindrical channel, see Fig. 1. We will denote the radius of the drop surface by R_s, and the inner radius of the pore—by R_p. To describe the process of drop formation, we will use cylindrical coordinates (r, z), where the z-axis coincides with the axis of rotational symmetry of the system, and the plane $z = 0$ coincides with the outer membrane surface (Fig. 1).

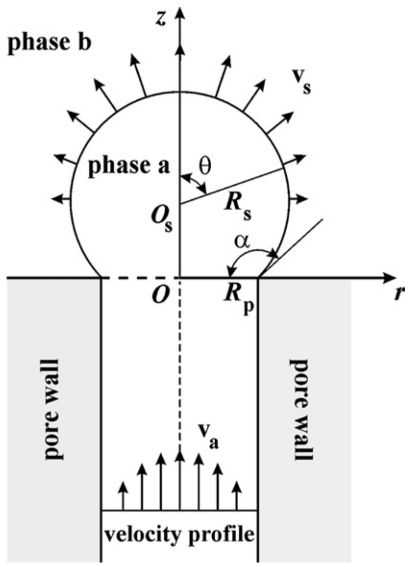

Fig. 1. Drop from the liquid phase 'a' growing at the orifice of a membrane pore. Phase 'b' is the outer liquid medium. R_p and R_s are, respectively, the radii of the cylindrical pore and spherical drop surface. The "protrusion" angle α characterizes the size of the drop ($0 \leqslant \alpha \leqslant 180°$), whereas the angle θ characterizes the positions of the material points at the drop surface; $\mathbf{v}_s$ is the surface velocity.

The inner and outer liquids will be referred as "phase a" and "phase b," respectively. For example, "phase a" could be oil and "phase b"—water, or vice versa. Due to the symmetry, the velocity fields, $\mathbf{v}_a$ and $\mathbf{v}_b$, in the respective phases can be expressed in the form:

$$\mathbf{v}_a = u_a \mathbf{e}_r + w_a \mathbf{e}_z, \qquad \mathbf{v}_b = u_b \mathbf{e}_r + w_b \mathbf{e}_z, \tag{2.1}$$

where $\mathbf{e}_r$ and $\mathbf{e}_z$ are the unit vectors of the r- and z-axes. Inside the cylindrical channel, far from its orifice, we have Poiseuille flow of the inner liquid [16]:

$$u_a = 0, \qquad w_a = 2v_m\left(1 - \frac{r^2}{R_p^2}\right) \quad \text{for } 0 \leqslant r \leqslant R_p \text{ and } z \to -\infty. \tag{2.2}$$

Here v_m is the mean velocity, and the subscript "a" denotes the inner liquid phase. The flow rate, Q, of the inner liquid is

$$Q = \pi R_p^2 v_m = \frac{dV}{dt}, \tag{2.3}$$

where V is the volume of the growing drop, and t is time. The volume can be expressed in the form:

$$V = \frac{\pi R_p^3}{3} \frac{2 + \cos\alpha}{(1 + \cos\alpha)^2} \sin\alpha, \tag{2.4}$$

where the angle α characterizes the protrusion of the droplet from the pore (Fig. 1), and will be termed below "protrusion angle." The differentiation of Eq. (2.4), in view of Eq. (2.3), yields:

$$\frac{d\alpha}{dt} = \frac{v_m}{R_p}(1 + \cos\alpha)^2. \tag{2.5}$$

The time derivative of the drop radius, R_s, is

$$\frac{dR_s}{dt} = \frac{d}{dt}\left(\frac{R_p}{\sin\alpha}\right) = -v_m \frac{1+\cos\alpha}{1-\cos\alpha}\cos\alpha. \tag{2.6}$$

Likewise, for the z-coordinate of the drop center, z_d, we obtain

$$\frac{dz_d}{dt} = -\frac{d}{dt}(R_p \cot\alpha) = v_m \frac{1+\cos\alpha}{1-\cos\alpha}. \tag{2.7}$$

The spherical drop surface obeys the equation

$$F(\mathbf{r}_s, t) \equiv r_s^2 + (z_s - z_d)^2 - R_s^2 = 0, \tag{2.8}$$

where (r_s, z_s) are the coordinates of a material point on the drop surface with respect to the immobile cylindrical coordinate system bound to the channel of the pore (Fig. 1); $\mathbf{r}_s$ is the position vector bound to this material point. In view of Eq. (2.8), the material derivative of the function F $(\mathbf{r}_s, t)$ should be equal to zero [17–19]:

$$\frac{\partial F}{\partial t} + \mathbf{v}_f \cdot \nabla F = 0, \quad f = a, b, \tag{2.9}$$

where ∇ is the spatial gradient operator. Substituting Eq. (2.8) into Eq. (2.9), one derives the following relationship at the drop surface:

$$\frac{r_s}{R_s} u_f + \frac{z_s - z_d}{R_s} w_f = \frac{dR_s}{dt} + \frac{z_s - z_d}{R_s}\frac{dz_d}{dt}, \quad f = a, b. \tag{2.10}$$

It is convenient to introduce polar coordinates:

$$r_s = R_s \sin\theta, \qquad z_s = z_d + R_s \cos\theta, \tag{2.11}$$

where θ is the polar angle that characterizes the position of the surface material points (Fig. 1). Further, with the help of Eqs. (2.1), (2.10), and (2.11) we deduce the following expression for the normal projection of the surface velocity with respect to the drop surface:

$$\mathbf{n} \cdot \mathbf{v}_s = \mathbf{n} \cdot \mathbf{v}_f = v_m \frac{1+\cos\alpha}{1-\cos\alpha}(\cos\theta - \cos\alpha), \quad f = a, b, \tag{2.12}$$

where $\mathbf{n}$ is the running unit normal to the drop surface:

$$\mathbf{n} = \mathbf{e}_r \sin\theta + \mathbf{e}_z \cos\theta. \tag{2.13}$$

The magnitude of the normal component of surface velocity, calculated from Eq. (2.12), is illustrated in Fig. 2. As it could be expected, the normal surface velocity has a maximum at the apex of the drop surface, where $\theta = 0$ and $\mathbf{n} \cdot \mathbf{v}_f / v_m = 1 + \cos\alpha$, and decreases with the increase of the protrusion angle, α (Figs. 2a and 2b).

3. Basic hydrodynamic equations and boundary conditions

The formation and detachment of micrometer-sized drops during membrane emulsification occurs at small values of the Reynolds number. To check that, we present Eq. (2.3) in the form $\pi R_p^2 v_m \approx 4\pi R_d^3/(3\Delta t)$, where Δt is the period of drop formation and R_d is the radius of the detached drop. Then, the Reynolds number could be estimated as Re $=$ $\rho v_m R_p/\eta \approx 4\rho R_d^3/(3\eta R_p \Delta t)$, where η is the dynamic viscosity of the liquid. Substituting typical parameter values: density $\rho = 1$ g/cm^3; dynamic viscosity $\eta = 0.01$ poises, $\Delta t = 0.1$ s; $R_d \approx 3R_p$, and $R_p \leqslant 20$ μm, one obtains Re ≈ 0.14. Hence, the Reynolds number is small and the classical Stokes equations can be used to describe the flow in the inner and outer liquid phases [20,21]:

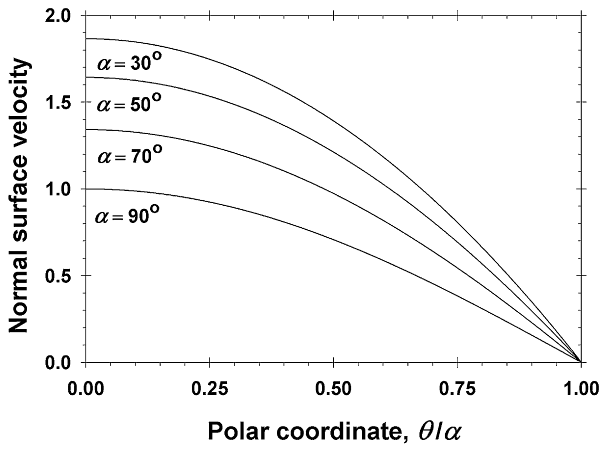

(a)

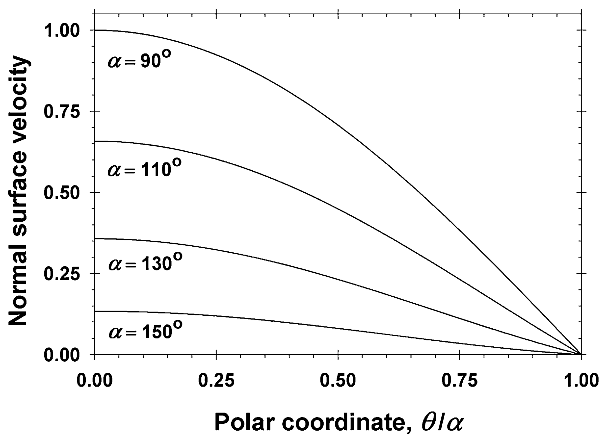

(b)

Fig. 2. The normal projection of the dimensionless surface velocity, $\mathbf{n} \cdot \mathbf{v}_s / v_m$, plotted vs the polar angle, θ, for different values of the protrusion angle: (a) $\alpha \leqslant 90°$, (b) $\alpha \geqslant 90°$.

$$\nabla \cdot \mathbf{v}_f = 0, \qquad \nabla p_f = \eta_f \nabla^2 \mathbf{v}_f, \quad f = a, b. \tag{3.1}$$

As usual p, $\mathbf{v}$, and η stand for pressure, velocity, and dynamic viscosity; the subscripts "a" and "b" denote quantities related to the inner and outer liquid phases, respectively (see Fig. 1).

It is convenient to introduce dimensionless variables, denoted by tilde, as follows:

$$r \equiv R_p \tilde{r}, \qquad z \equiv R_p \tilde{z}, \qquad \mathbf{v}_a \equiv v_m \tilde{\mathbf{v}}_a, \qquad \mathbf{v}_b \equiv v_m \tilde{\mathbf{v}}_b, \tag{3.2}$$

$$p_a \equiv p_\infty + \frac{2\sigma}{R_s} + \frac{\eta_a v_m}{R_p}\tilde{p}_a, \qquad p_b \equiv p_\infty + \frac{\eta_b v_m}{R_p}\tilde{p}_b, \tag{3.3}$$

where p_∞ is the equilibrium bulk pressure in the outer phase far from the forming drop; σ is the oil/water interfacial tension. With the help of Eqs. (2.1), (3.2), and (3.3), we bring the system of equations (3.1) in the form [20,21]:

$$\frac{1}{\tilde r}\frac{\partial}{\partial \tilde r}(\tilde r\tilde u_{\rm f})+\frac{\partial \tilde w_{\rm f}}{\partial \tilde z}=0, \tag{3.4}$$

$$\frac{\partial}{\partial \tilde r}\left[\frac{1}{\tilde r}\frac{\partial}{\partial \tilde r}(\tilde r\tilde u_{\rm f})\right]+\frac{\partial^2 \tilde u_{\rm f}}{\partial \tilde z^2}=\frac{\partial \tilde p_{\rm f}}{\partial \tilde r}, \tag{3.5}$$

$$\frac{1}{\tilde r}\frac{\partial}{\partial \tilde r}\left(\tilde r\frac{\partial \tilde w_{\rm f}}{\partial \tilde r}\right)+\frac{\partial^2 \tilde w_{\rm f}}{\partial \tilde z^2}=\frac{\partial \tilde p_{\rm f}}{\partial \tilde z}, \tag{3.6}$$

where $\mathrm{f}=\mathrm{a}, \mathrm{b}$. Equations (3.4)–(3.6), along with the respective boundary conditions (see below), form a system of equations for determining $\tilde p_{\rm f}$, $\tilde u_{\rm f}\equiv u_{\rm f}/v_{\rm m}$, and $\tilde w_{\rm f}\equiv w_{\rm f}/v_{\rm m}$. To obtain a single partial differential equation for the considered problem, we apply a standard hydrodynamic approach that is based on introducing a dimensionless stream function, $\psi_{\rm f}$, as follows [20,21]:

$$\tilde u_{\rm f}\equiv \frac{\partial \psi_{\rm f}}{\partial \tilde z},\qquad \tilde w_{\rm f}\equiv -\frac{1}{\tilde r}\frac{\partial}{\partial \tilde r}(\tilde r\psi_{\rm f}),\qquad \mathrm{f}=\mathrm{a},\mathrm{b}. \tag{3.7}$$

In view of Eq. (3.7), the continuity equation (3.4) is automatically satisfied and the stream function obeys the equation [20,21]:

$$L\big[L(\psi_{\rm f})\big]=0,\qquad \mathrm{f}=\mathrm{a},\mathrm{b}, \tag{3.8}$$

where the linear differential operator L is defined as

$$L(f)\equiv \frac{\partial}{\partial \tilde r}\left[\frac{1}{\tilde r}\frac{\partial}{\partial \tilde r}(\tilde r f)\right]+\frac{\partial^2 f}{\partial \tilde z^2}, \tag{3.9}$$

where f is an arbitrary function. Note that the partial differential equation (3.8) is of the fourth order and two boundary conditions at each boundary are needed for its solution [17,20,21]. The pressure, $\tilde p_{\rm f}$, $\mathrm{f}=\mathrm{a},\mathrm{b}$, is simply related to the stream function, $\psi_{\rm f}$, through the basic Stokes equations (3.5) and (3.6).

An important step in the modeling of the drop expansion is to transform the hydrodynamic boundary conditions in the terms of the stream function.

At the axis of symmetry, $\tilde r=0$, the radial velocity, $u_{\rm f}$, and the curl of the liquid flow must be zero, irrespective of the value of z. Therefore, the stream function must be an odd function of r [20,21], and the following boundary conditions take place:

$$\psi_{\rm f}=0,\qquad \frac{\partial^2 \psi_{\rm f}}{\partial \tilde r^2}=0\quad \text{at } \tilde r=0,\qquad \mathrm{f}=\mathrm{a},\mathrm{b}. \tag{3.10}$$

Inside the channel of the pore, far from its orifice, we have Poiseuille flow with a parabolic velocity profile given by Eq. (2.2). Then, from Eqs. (2.2), (3.2), and (3.7) we derive

$$\psi_{\rm a}=\frac{\tilde r^3}{2}-\tilde r,\qquad \frac{\partial \psi_{\rm a}}{\partial \tilde z}=0\quad \text{at } 0\leqslant \tilde r\leqslant 1 \text{ and } \tilde z\to -\infty. \tag{3.11}$$

At the solid wall of the cylindrical pore ($\tilde r=1$, see Fig. 1), we must have $u_{\rm a}=w_{\rm a}=0$. Substituting $\tilde r=1$ in Eq. (3.11), we get $\psi_{\rm a}=-1/2$. Further, we substitute the latter relationships in the expression for $\tilde w_{\rm f}$ in Eq. (3.7) to derive:

$$\psi_{\rm a}=-\frac{1}{2},\qquad \frac{\partial \psi_{\rm a}}{\partial \tilde r}=\frac{1}{2}\quad \text{at } \tilde r=1 \text{ and } \tilde z\leqslant 0. \tag{3.12}$$

Likewise, we have $u_{\rm b}=w_{\rm b}=0$ at the solid surface $\tilde z=0$ for $\tilde r\geqslant 1$, which represents the boundary of the membrane with the outer liquid (Fig. 1). For this boundary, we obtain

$$\psi_{\rm b}=-\frac{1}{2\tilde r},\qquad \frac{\partial \psi_{\rm b}}{\partial \tilde z}=0\quad \text{at } \tilde r\geqslant 1 \text{ and } \tilde z=0. \tag{3.13}$$

Here, we have used the fact that the substitution of $\psi_{\rm b}\propto 1/\tilde r$ into Eq. (3.7) yields $\tilde w_{\rm f}=0$; the constant of proportionality is determined from the condition $\psi_{\rm b}=\psi_{\rm a}=-1/2$ at $\tilde r=1$, see Eq. (3.12).

At the drop surface we impose the kinematic boundary condition given by Eq. (2.12); thus, we derive (Appendix A in Supplementary material):

$$\psi_{\rm a}=\psi_{\rm b}=\frac{(1+\cos\alpha)\sin\theta}{(1-\cos\alpha)\sin\alpha}\left(\frac{\cos\alpha}{1+\cos\theta}-\frac{1}{2}\right)\quad \text{at the drop surface.} \tag{3.14}$$

It is important to note that the stream function (3.14) is continuous at the edge of the pore, i.e., the value of $\psi_{\rm f}$ is equal to $-1/2$ at $\theta=\alpha$, see also Eqs. (3.12) and (3.13).

At the oil–water interface, the tangential components of the velocities in the two phases should be equal, $\mathbf{t}\cdot\mathbf{v}_{\rm a}=\mathbf{t}\cdot\mathbf{v}_{\rm b}$ [16]; here, $\mathbf{t}$ is a running unit tangent to the drop surface. In the case of membrane emulsification, a high concentration of surfactant is used to stabilize the obtained emulsion droplets. The adsorbed surfactant molecules give rise to a considerable surface elasticity (Marangoni–Gibbs effect) and surface viscosity, which have to be taken into account in the tangential stress balance [18,19,22]. It has been proven both experimentally and theoretically [18,22–24] that the surface (Gibbs) elasticity and viscosity damp the surface mobility even at very low surfactant concentrations. Therefore, we could treat the oil–water interface as tangentially immobile, i.e., $\mathbf{t}\cdot\mathbf{v}_{\rm a}=\mathbf{t}\cdot\mathbf{v}_{\rm b}=0$ at the drop surface. The tangential immobility leads to a boundary condition of Neumann type for the stream function (see Appendix A in Supplementary material):

$$\frac{\partial \psi_{\rm f}}{\partial n}+\psi_{\rm f}\sin\alpha=0\quad \text{at the drop surface}, \tag{3.15}$$

where $\mathrm{f}=\mathrm{a},\mathrm{b}$. The directional derivative in Eq. (3.15) is

$$\frac{\partial \psi_{\rm f}}{\partial n}=\mathbf{n}\cdot\nabla\psi_{\rm f}=\sin\theta\frac{\partial \psi_{\rm f}}{\partial \tilde r}+\cos\theta\frac{\partial \psi_{\rm f}}{\partial \tilde z}. \tag{3.16}$$

In view of Eqs. (3.15) and (3.16), the problem splits into two separate boundary problems in the phases "a" and "b."

4. Solution of the problem in curvilinear coordinates

The hydrodynamic equations (3.8) for the stream functions $\psi_{\rm a}$ and $\psi_{\rm b}$, along with the respective boundary conditions (3.10)–(3.15), have no analytical solution. To solve the problem numerically, we parameterized the three spatial domains of the considered system by means of appropriate curvilinear coordinates (Section 4.1). The derived equations are reformulated in terms of the new coordinates (Section 4.2). The obtained numerical results for the stream function and velocity components are presented and discussed in Section 4.3.

4.1. Coordinate transformations

It is convenient to transform the physical space, occupied by the two liquid phases, including the emulsion drop, into a finite

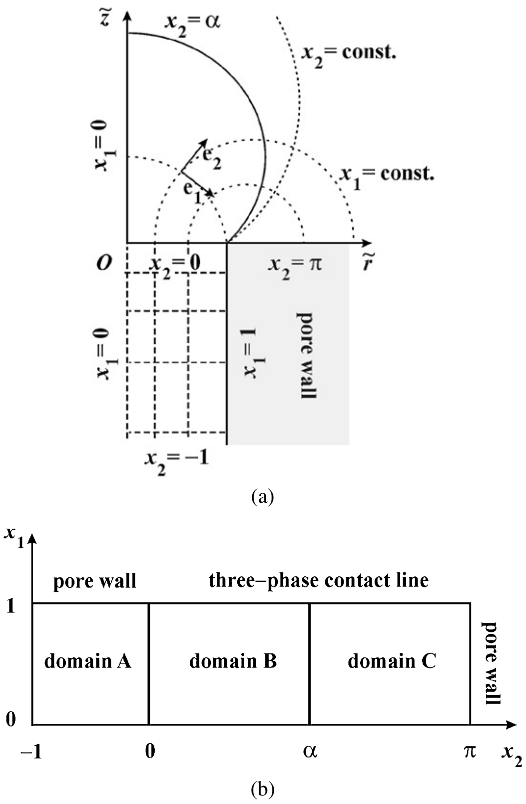

Fig. 3. (a) Curvilinear coordinates (x_1, x_2) introduced in Section 4. (b) The pore interior, the drop interior and the outer phase are transformed into the rectangular domains A, B, and C, respectively.

rectangular domain. For this goal, we consider three separate domains (Fig. 3). Domain A represents the interior of the cylindrical capillary. Domain B is the interior of the emulsion drop. Domain C is the outer liquid (the continuous phase of the emulsion).

In the domain A, it is convenient to replace the cylindrical coordinates $(\tilde{r}, \tilde{z})$ by curvilinear coordinates (x_1, x_2), defined as follows:

$$x_1 \equiv \tilde{r}, \qquad x_2 \equiv \frac{\tilde{z}}{1-\tilde{z}}. \tag{4.1}$$

Thus, the domain corresponding to $0 \leqslant \tilde{r} \leqslant 1$ and $\tilde{z} \leqslant 0$, is transformed into a finite rectangle, for which $0 \leqslant x_1 \leqslant 1$ and $-1 \leqslant x_2 \leqslant 0$ (Fig. 3). The coordinate surfaces $x_1 = \text{const.}$ are vertical cylinders, whereas the coordinate surfaces $x_2 = \text{const.}$ are horizontal planes. Using the curvilinear coordinates defined by Eq. (4.1), we derive

$$\frac{\partial f}{\partial \tilde{r}} = \frac{\partial f}{\partial x_1}, \qquad \frac{\partial f}{\partial \tilde{z}} = (1+x_2)^2 \frac{\partial f}{\partial x_2}. \tag{4.2}$$

Because the domains B and C are separated by a spherical phase boundary (the drop surface), it is convenient to introduce orthogonal toroidal coordinates in these two regions:

$$\tilde{r} \equiv \frac{2x_1}{h}, \qquad \tilde{z} \equiv \frac{1-x_1^2}{h} \sin x_2, \tag{4.3}$$

$$h \equiv 1 + x_1^2 + \left(1 - x_1^2\right) \cos x_2. \tag{4.4}$$

The coordinates x_1 and x_2, defined by Eqs. (4.3)–(4.4), are similar to the conventional toroidal coordinates [25–27]. In our case, the coordinate surfaces $x_1 = \text{const.}$ are toroids, whereas the surfaces $x_2 = \text{const.}$ are spheres (Fig. 3). The latter obey the equation:

$$\tilde{r}^2 + \left(\tilde{z} + \cot x_2\right)^2 = \frac{1}{\sin^2 x_2}. \tag{4.5}$$

One could check that (irrespective of the value of x_2) all spheres described by Eq. (4.5) are passing through the circumference $\tilde{r} = 1$, $\tilde{z} = 0$, which is the edge at the orifice of the pore. Because the drop surface represents a sphere of dimensionless radius $\tilde{R}_s \equiv R_s/R_p = 1/\sin\alpha$ (Fig. 1), from Eq. (4.5) we find that $x_2 = \alpha$ at the drop surface (at the boundary between the domains B and C). In addition, the boundary between the domains A and B corresponds to $x_2 = 0$; see Eqs. (4.1) and (4.3) and Fig. 3. Thus, the domain B represents a rectangle, for which $0 \leqslant x_1 \leqslant 1$ and $0 \leqslant x_2 \leqslant \alpha$, whereas for the domain C we have $0 \leqslant x_1 \leqslant 1$ and $\alpha \leqslant x_2 \leqslant \pi$.

From the definition of the toroidal coordinates (4.3) and (4.4), it follows that

$$\frac{\partial \tilde{r}}{\partial x_1} = \frac{2}{h^2}\left[\left(1-x_1^2\right) + \left(1+x_1^2\right)\cos x_2\right],$$

$$\frac{\partial \tilde{z}}{\partial x_2} = \frac{1-x_1^2}{2} \frac{\partial \tilde{r}}{\partial x_1}, \tag{4.6}$$

$$\frac{\partial \tilde{r}}{\partial x_2} = \frac{2}{h^2} x_1 \left(1-x_1^2\right) \sin x_2, \qquad \frac{\partial \tilde{z}}{\partial x_1} = -\frac{2}{1-x_1^2} \frac{\partial \tilde{r}}{\partial x_2}. \tag{4.7}$$

The respective metric (Lamé) coefficients are [25,26]:

$$h_1 = \frac{2}{h}, \qquad h_2 = \frac{1-x_1^2}{h}. \tag{4.8}$$

Two other useful relationships connect the derivatives in terms of the cylindrical and toroidal coordinates:

$$\frac{\partial f}{\partial \tilde{r}} = \frac{1}{2}\left[\left(1-x_1^2\right) + \left(1+x_1^2\right)\cos x_2\right] \frac{\partial f}{\partial x_1} + \frac{2x_1 \sin x_2}{1-x_1^2} \frac{\partial f}{\partial x_2}, \tag{4.9}$$

$$\frac{\partial f}{\partial \tilde{z}} = -x_1 \sin x_2 \frac{\partial f}{\partial x_1} + \left(1 + \frac{1+x_1^2}{1-x_1^2} \cos x_2\right) \frac{\partial f}{\partial x_2}. \tag{4.10}$$

The introduced curvilinear coordinates are convenient, because the boundary conditions are imposed on coordinate surfaces. In the next sections, we specify the form of the differential equations and boundary conditions for the domains A, B, and C.

4.2. Hydrodynamic equations and boundary conditions in curvilinear coordinates

As mentioned above, the domain A is a rectangle for which $0 \leqslant x_1 \leqslant 1$ and $-1 \leqslant x_2 \leqslant 0$ (Fig. 3). In this domain, the linear differential operator L, defined by Eq. (3.9), acquires the form:

$$L(f) = \frac{\partial^2 f}{\partial x_1^2} + (1+x_2)^4 \frac{\partial^2 f}{\partial x_2^2} + \frac{1}{x_1}\frac{\partial f}{\partial x_1} + 2(1+x_2)^3 \frac{\partial f}{\partial x_2} - \frac{f}{x_1^2}. \tag{4.11}$$

In the domain A, the stream function ψ_a satisfies Eq. (3.8), where the linear differential operator L is given by Eq. (4.11).

Furthermore, with the help of Eqs. (4.3), (4.4), (4.9), and (4.10), one can express the differential operator L in terms of the toroidal coordinates (x_1, x_2):

$$L(f) = \frac{1}{h_1^2}\frac{\partial^2 f}{\partial x_1^2} + \frac{1}{h_2^2}\frac{\partial^2 f}{\partial x_2^2} + \left(\frac{h}{2x_1} - \frac{2x_1}{1-x_1^2}\right)\frac{1}{h_1}\frac{\partial f}{\partial x_1} + \frac{\sin x_2}{h_2}\frac{\partial f}{\partial x_2} - \frac{f}{h_1^2 x_1^2}. \tag{4.12}$$

In the domains B and C, the stream functions ψ_a and ψ_b satisfy Eq. (3.8), in which the linear differential operator L is given by Eq. (4.12).

At the axis of symmetry, $\tilde{r} = 0$, which corresponds to $x_1 = 0$, the stream function is an odd function of x_1 [20,21], and the boundary conditions (3.10) reduce to

$$\psi_f = 0, \qquad \frac{\partial^2 \psi_f}{\partial x_1^2} = 0 \quad \text{at } x_1 = 0 \text{ and } -1 \leqslant x_2 \leqslant 0, \quad \text{f} = \text{a, b}. \tag{4.13}$$

In the interior of the capillary channel, far from its orifice, we have $\tilde{z} \to -\infty$ and $x_2 = -1$. Then, from the boundary condition, Eq. (3.11), using Eq. (4.1) we derive

$$\psi_a = \frac{x_1^3}{2} - x_1, \qquad \frac{\partial \psi_a}{\partial x_2} = 0 \quad \text{at } 0 \leqslant x_1 \leqslant 1 \text{ and } x_2 = -1. \tag{4.14}$$

The second relation in Eq. (4.14) follows from the fact that the perturbations of the Poiseuille flow in cylindrical channels decay exponentially with the distance z [20,21]. Therefore, $\partial\psi_a/\partial\tilde{z}$ decays faster for $\tilde{z} \to -\infty$ than $(1+x_2)^2$ for $x_2 \to -1$.

The solid wall of the cylindrical channel corresponds to $\tilde{r} = x_1 = 1$. With the help of the definitions in Eq. (4.1), the respective boundary conditions, Eq. (3.12), can be rewritten in the form:

$$\psi_a = -\frac{1}{2}, \qquad \frac{\partial \psi_a}{\partial x_1} = \frac{1}{2} \quad \text{at } x_1 = 1 \text{ and } -1 < x_2 \leqslant 0. \tag{4.15}$$

At the outer membrane wall, where $\tilde{z} = 0$ and $x_2 = \pi$ (Fig. 3), with the help of Eqs. (3.13), (4.3), (4.4), and (4.10), we derive the following boundary conditions:

$$\psi_b = -\frac{x_1}{2}, \qquad \frac{\partial \psi_b}{\partial x_2} = 0 \quad \text{at } 0 \leqslant x_1 \leqslant 1 \text{ and } x_2 = \pi. \tag{4.16}$$

At the drop surface (the oil–water interface), we have $x_2 = \alpha$. With the help of Eqs. (4.3) and (4.4), after some mathematical transformations one can express boundary conditions, Eqs. (3.14) and (3.15), in the form (Appendix B in Supplementary material):

$$\psi_f = -\frac{x_1}{h}\left[1 + \left(1 - x_1^2\right)\cos\alpha\right] \quad \text{at } x_2 = \alpha \text{ and } 0 \leqslant x_1 \leqslant 1, \tag{4.17}$$

$$\frac{1}{h_2}\frac{\partial \psi_f}{\partial x_2} + \psi_f \sin\alpha = 0 \quad \text{at } x_2 = \alpha \text{ and } 0 \leqslant x_1 \leqslant 1, \tag{4.18}$$

where f = a, b.

The present formulation of the problem introduces two additional boundaries (Fig. 3b): (i) The circumference of the pore edge, which is the point (1, 0) in cylindrical coordinates $(\tilde{r}, \tilde{z})$, in curvilinear coordinates is expanded in the segment $x_1 = 1$ and $0 \leqslant x_2 \leqslant \pi$ of the domains B and C. (ii) The domains A and B at $x_2 = 0$ are separated by an imaginary boundary, which appears because of the used different coordinates and the respective different forms of the differential operator L given by Eqs. (4.11) and (4.12).

At the edge of the pore, the values of the stream functions are determined from Eqs. (4.15) and (4.16). In addition, using the nonslip boundary condition one derives (Appendix B in Supplementary material):

$$\psi_f = -\frac{1}{2}, \qquad \frac{\partial \psi_f}{\partial x_1} = \frac{\cos x_2}{2} \quad \text{at } x_1 = 1,\ 0 \leqslant x_2 \leqslant \pi, \quad \text{and f} = \text{a, b}. \tag{4.19}$$

To have a continuous stream function at the boundary between the domains A and B, the values of ψ_a and its z-derivatives on both sides of the boundary must be equal. To fulfill this requirement, it is enough to have

$$\{\psi_a\} = 0, \qquad \left\{\frac{\partial \psi_a}{\partial \tilde{z}}\right\} = 0, \qquad \left\{\frac{\partial^2 \psi_a}{\partial \tilde{z}^2}\right\} = 0, \qquad \left\{\frac{\partial^3 \psi_a}{\partial \tilde{z}^3}\right\} = 0 \quad \text{at } 0 \leqslant \tilde{r} \leqslant 1, \tag{4.20}$$

where $\{f\}$ means the jump of the respective function across the boundary:

$$\{f\} \equiv f\big|_{\tilde{z}\to 0+0} - f\big|_{\tilde{z}\to 0-0}. \tag{4.21}$$

In terms of the introduced coordinates, the derivatives in Eq. (4.20), calculated in the domains A and B have a different forms. After some mathematical transformations, the boundary conditions (4.20) can be represented in the form (Appendix C in Supplementary material):

$$\left.\frac{\partial \psi_a}{\partial x_2}\right|_{x_2=0-0} = \frac{2}{1-x_1^2}\left.\frac{\partial \psi_a}{\partial x_2}\right|_{x_2=0+0}, \tag{4.22}$$

$$\left.\left(\frac{\partial^2 \psi_a}{\partial x_2^2} + 2\frac{\partial \psi_a}{\partial x_2}\right)\right|_{x_2=0-0} = \left.\left[\frac{4}{(1-x_1^2)^2}\frac{\partial^2 \psi_a}{\partial x_2^2} - \frac{2x_1}{1-x_1^2}\frac{\partial \psi_a}{\partial x_1}\right]\right|_{x_2=0+0}, \tag{4.23}$$

$$\left.\left(\frac{\partial^3 \psi_a}{\partial x_2^3} + 6\frac{\partial^2 \psi_a}{\partial x_2^2} + 6\frac{\partial \psi_a}{\partial x_2}\right)\right|_{x_2=0-0} = \left.\left[\frac{8}{(1-x_1^2)^3}\frac{\partial^3 \psi_a}{\partial x_2^3} - \frac{12x_1}{(1-x_1^2)^2}\frac{\partial^2 \psi_a}{\partial x_1 \partial x_2} - \frac{4(1+3x_1^2)}{(1-x_1^2)^3}\frac{\partial \psi_a}{\partial x_2}\right]\right|_{x_2=0+0}. \tag{4.24}$$

We solved numerically the partial differential equations, Eqs. (3.8), in which the linear differential operator L is defined by Eqs. (4.11) and (4.12), using the boundary conditions (4.13)–(4.19) and (4.22)–(4.24). For this purpose, in each of the domains A, B, and C a regular numerical grid of 101 × 101 points was introduced. The derivatives appearing in the equations and boundary conditions were replaced by their finite difference approximations of the second order [25,28–31]. The resulting system of linear equations was solved by means of a direct algorithm developed by us, which gives the exact solution in the frame of the computer's double precision. Thus, the problem was solved by one step, without iterations.

4.3. Results for the velocity field

The numerical solution of the boundary problem yields the stream function, and the two components of velocity in each phase: $\psi_f(x_1,\ x_2)$, $\tilde{u}_f(x_1,\ x_2)$, and $\tilde{w}_f(x_1,\ x_2)$, f = a, b. First, the stream functions, ψ_a and ψ_b, are computed. Next, the radial and z-components of velocity, $\tilde{u}_f$ and $\tilde{w}_f$, f = a, b, are calculated by using Eqs. (3.7) and (4.2) in the domain A,

$$\tilde{u}_a = (1+x_2)^2\frac{\partial\psi_a}{\partial x_2},\qquad \tilde{w}_a = -\frac{\partial\psi_a}{\partial x_1} - \frac{\psi_a}{x_1}, \tag{4.25}$$

and by using Eqs. (3.7), (4.3), (4.9), and (4.10) in the domains B and C:

$$\tilde{u}_f = -x_1\sin x_2\frac{\partial\psi_f}{\partial x_1} + \left(1+\frac{1+x_1^2}{1-x_1^2}\cos x_2\right)\frac{\partial\psi_f}{\partial x_2}, \tag{4.26}$$

$$\tilde{w}_f = -\frac{1}{2}\Big[\big(1-x_1^2\big)+\big(1+x_1^2\big)\cos x_2\Big]\frac{\partial\psi_f}{\partial x_1} - \frac{2x_1\sin x_2}{1-x_1^2}\frac{\partial\psi_f}{\partial x_2} - \frac{h}{2x_1}\psi_f, \tag{4.27}$$

where f = a, b. The derivatives appearing in Eqs. (4.25)–(4.27) are determined numerically from computed values of ψ_f, f = a, b, in the domains A, B, and C, using the respective finite difference approximations of the second order [25,28–31].

Illustrative contour plots of the z-component of velocity, w_f, are shown in Fig. 4 for $\alpha = 30°, 90°$, and $150°$. The vertical dashed lines in Figs. 4a, 4b, and 4c represent the boundaries between the domains A, B, and C; see Fig. 3. As it could be expected, w_f is maximal at the axis of symmetry ($x_1 = 0$). Moreover, w_f decreases with the distance from the capillary tip in the domains B and C. The role of the drop surface on the flow inside the capillary (in the domain A) is more pronounced for small values of the protrusion angle (Fig. 4a). For $\alpha \geqslant 90°$, the flow in the capillary does not deviate considerably from the Poisseuille flow (Figs. 4b and 5c). In addition, for $\alpha = 90°$ w_f exhibits a significant change at the oil–water interface. For $\alpha > 90°$ the magnitude of w_f at the drop surface is small and decreases with the increase of α. However, the integral effect of w_f on the hydrodynamic drag force acting on the drop surface is not negligible because of the increase of the interfacial area (see Section 5).

Contour plot diagrams of the radial velocity component, $\tilde{u}_f$, f = a, b, are shown in Fig. 5 for protrusion angles $\alpha = 30°, 90°$, and $150°$. For $\alpha = 30°$ (Fig. 5a), the radial component of the velocity has a shallow minimum inside the capillary; its negative value means that the radial projection of velocity is directed toward the axis of symmetry. In this region, the radial component is much smaller than the z-component, $|u_a/w_a| \leqslant 0.02$. For $\alpha < 90°$, the maximum of $\tilde{u}_f$ is located in the outer phase, domain C (Fig. 5a). For $\alpha = 90°$, the maximum of $\tilde{u}_f$ is on the drop surface (Fig. 5b), whereas for $\alpha = 150°$ this maximum is located inside the drop (Fig. 5c). Moreover, for $\alpha \geqslant 90°$, the radial velocity component $\tilde{u}_f$ is positive in the whole region, i.e., and the velocity vector is always tilted outwards with respect to the axis of symmetry. Note also that for $\alpha = 90°$ (Fig. 5b), the maximum of $\tilde{u}_f$ at the capillary tip is about 0.02, whereas for $\alpha = 150°$ (Fig. 5c) it increases up to about 0.18.

The toroidal coordinates (x_1, x_2) are convenient for numerical calculations, and the contour plots (Figs. 4 and 5) are useful for estimating the magnitudes of the stream function and velocity components. However, these curvilinear coordinates are not convenient for spatial presentation of the flow pattern, because they distort the shape of the real system. For this reason, in Fig. 6 we show the velocity vector, **v**, recalculated in the conventional Cartesian coordinates; as usual, the z-axis coincides with the axis of symmetry of the system. The drop in Fig. 6 corresponds to $R_s/R_p = 1/\sin\alpha = 2/\sqrt{3}(\alpha = 120°)$. The general pattern of the velocity field in Fig. 6 does not indicate existence of vorticity structures inside the drop (symmetric curls on the left and right of the z-axis in Fig. 1), as expected under other physical conditions [32]. The flow is predominantly directed along the z-axis, out of the pore, with a superimposed additional radial flow, engendered by the radial expansion of the drop surface. The flow pattern is similar (without vorticity structures in the drop) also for the other values of α. We recall that the used boundary conditions at the drop surface, Eqs. (2.12) and (3.15), physically correspond to a *tangentially immobile* oil–water interface. In other words, the displacement vector of the material points on the expanding drop surface is directed along the *normal* to this surface. Such a kinematic regime is expected when adsorbed surfactant molecules give rise to a considerable surface elasticity (Marangoni–Gibbs effect).

5. Hydrodynamic force acting on the emulsion drop

5.1. Hydrodynamic force coefficients

Our aim here is to calculate the hydrodynamic force, $\mathbf{F}_h$, acting on the drop. For this goal, we could formally consider the drop that is protruding from the capillary (Fig. 1) as being "solidified," and could integrate the pressure in the surrounding phases over the drop surface, S. The latter surface consists of the oil–water interface, i.e., the boundary S_{BC} between the domains B and C, and of the imaginary planar boundary S_{AB} between the domains A and B; S_{AB} separates the drop from the pore channel; see Fig. 3. Thus, $\mathbf{F}_h$ can be presented as a sum of contributions from the pressures in the phases "a" and "b":

$$\mathbf{F}_a = \int\limits_{S_{AB}} ds\,\mathbf{n}\cdot\left[\mathbf{P}_a - \left(p_\infty + \frac{2\sigma}{R_s}\right)\mathbf{U}\right],$$
$$\mathbf{F}_b = \int\limits_{S_{BC}} ds\,\mathbf{n}\cdot(\mathbf{P}_b - p_\infty\mathbf{U}), \tag{5.1}$$

where **U** is the spatial unit tensor; **n** is the outer running normal. In Eq. (5.1), we have subtracted the *static* pressure in the

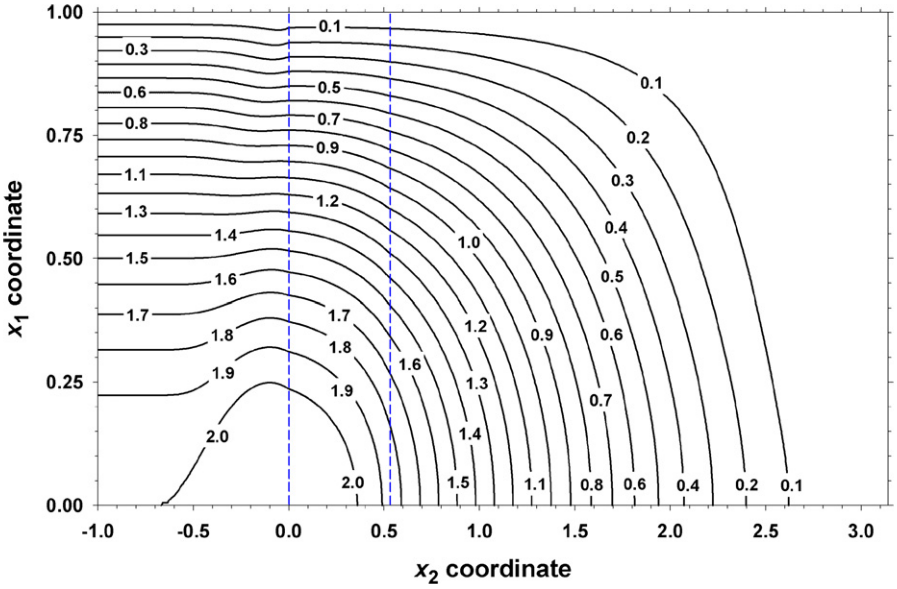

(a)

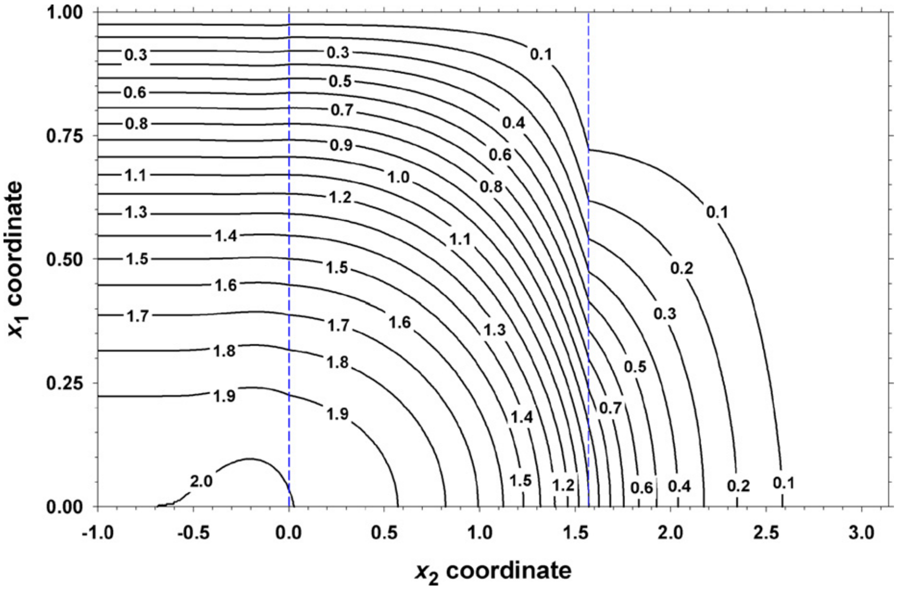

(b)

Fig. 4. Contour-plot diagrams of the dimensionless z-component of velocity, $\tilde{w}_{\mathrm{f}}(x_1, x_2)$, for different protrusion angles: (a) $\alpha = 30°$, (b) $\alpha = 90°$, (c) $\alpha = 150°$. The vertical dashed lines correspond to the boundaries between the domains A, B, and C in Fig. 3b.

respective phase from the pressure tensor. The pressure tensors, $\mathbf{P}_{\mathrm{a}}$ and $\mathbf{P}_{\mathrm{b}}$, are determined by the Newton's law for a viscous fluid [16–21]:

$$\mathbf{P}_{\mathrm{f}} \equiv p_{\mathrm{f}}\mathbf{U} - \eta_{\mathrm{f}}\left[\nabla \mathbf{v}_{\mathrm{f}} + (\nabla \mathbf{v}_{\mathrm{f}})^{\mathrm{tr}}\right], \quad \mathrm{f} = \mathrm{a}, \mathrm{b}, \tag{5.2}$$

where the superscript "tr" means transposition. The Stokes equations, Eq. (3.1), are equivalent to $\nabla \cdot \mathbf{P}_{\mathrm{f}} = 0$. Then, in accordance with the Gauss–Ostrogradsky theorem, the force $\mathbf{F}_{\mathrm{b}}$ given by Eq. (5.1) can be calculated at every mathematical surface that together with S_{BC} forms a closed surface; this is the Faxen theorem [20]. The calculation of $\mathbf{F}_{\mathrm{b}}$ is simpler if we choose the surface $z = 0$ at $r > R_{\mathrm{p}}$ as integration domain. Thus, both integrals in Eq. (5.1) are taken over portions of the plane $z = 0$: at $0 < r < R_{\mathrm{p}}$ for $\mathbf{F}_{\mathrm{a}}$, and at $R_{\mathrm{p}} < r < \infty$ for $\mathbf{F}_{\mathrm{b}}$:

$$\mathbf{F}_{\mathrm{a}} = 2\pi \mathbf{e}_z \int_0^{R_{\mathrm{p}}} \left(P_{\mathrm{a},zz} - p_\infty - \frac{2\sigma}{R_{\mathrm{s}}}\right) r\,dr, \tag{5.3}$$

$$\mathbf{F}_{\mathrm{b}} = 2\pi \mathbf{e}_z \int_{R_{\mathrm{p}}}^{\infty} (P_{\mathrm{b},zz} - p_\infty) r\,dr, \tag{5.4}$$

where the values of the tensorial components $P_{\mathrm{a},zz}$ and $P_{\mathrm{b},zz}$ are taken at $z = 0$. Because, $\mathbf{F}_{\mathrm{a}}$ and $\mathbf{F}_{\mathrm{b}}$ have purely hydrodynamic character, we could seek expressions for their magnitudes in the conventional Stokes form [16,20,21]:

$$F_{\mathrm{a}} = f_{\mathrm{a}}\eta_{\mathrm{a}} R_{\mathrm{p}} v_{\mathrm{m}}, \qquad F_{\mathrm{b}} = f_{\mathrm{b}}\eta_{\mathrm{b}} R_{\mathrm{p}} v_{\mathrm{m}}. \tag{5.5}$$

Of course, the coefficients, f_{a} and f_{b}, are, in general, different from 6π. Our aim below is to determine their values. For this

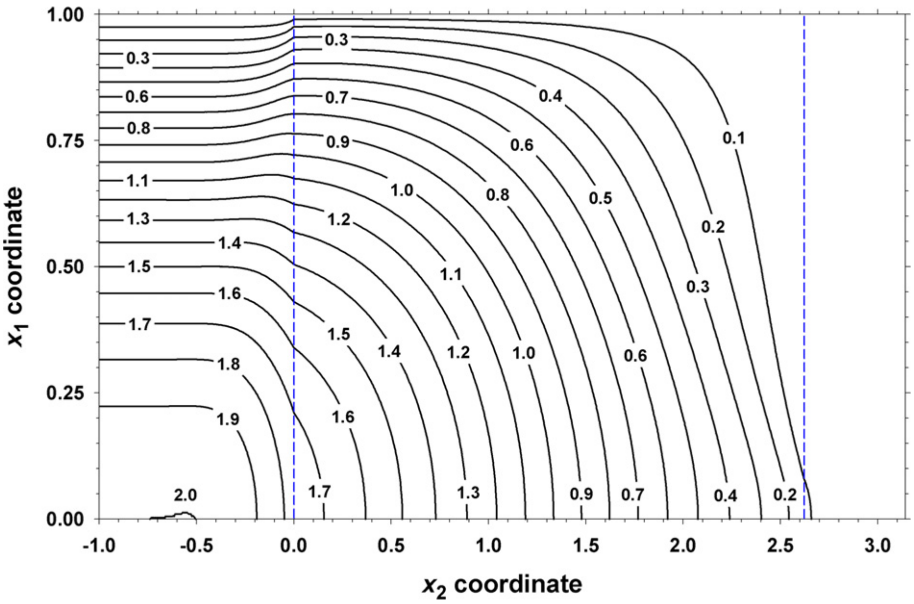

(c)

Fig. 4. *(continued)*

goal, we express $P_{f,zz}$ from Eq. (5.2) and use the continuity equation (3.1):

$$P_{f,zz} = p_f - 2\eta_f \frac{\partial w_f}{\partial z} = p_f + 2\eta_f \frac{1}{r}\frac{\partial}{\partial r}(r u_f), \quad f = a, b. \tag{5.6}$$

From the boundary conditions, we have $u_a(r = R_p) = u_b(r = R_p) = u_b(r \to \infty) = 0$. Therefore, when substituting Eq. (5.6) into Eqs. (5.3) and (5.4), and integrating, the last term in Eq. (5.6) gives zero contribution and the obtained results read:

$$F_a = 2\pi \int_0^{R_p} \left(p_a - p_\infty - \frac{2\sigma}{R_s}\right) r\,dr \quad \text{at } z = 0, \tag{5.7}$$

$$F_b = 2\pi \int_{R_p}^{\infty} (p_b - p_\infty) r\,dr \quad \text{at } z = 0. \tag{5.8}$$

Finally, in Eqs. (5.7) and (5.8) we introduce dimensionless variables in accordance with Eq. (3.3). As a result, we obtain Eq. (5.5), where the dimensionless coefficients of the hydrodynamic force are given by the expressions:

$$f_a = 2\pi \int_0^1 \tilde{p}_a \tilde{r}\,d\tilde{r}, \qquad f_b = 2\pi \int_1^{\infty} \tilde{p}_b \tilde{r}\,d\tilde{r} \quad \text{at } z = 0. \tag{5.9}$$

To determine the pressures p_a and p_b in the phases 'a' and 'b,' we need two boundary conditions. In the bulk of phase 'b' this is the condition $p_b \to p_\infty$. To obtain the respective boundary condition in the phase 'a,' we will use the Laplace equation of capillarity. For this goal, we present p_a and p_b in the form:

$$p_a \equiv p_\infty + \frac{2\sigma}{R_s} + p_{a,dyn}, \qquad p_b \equiv p_\infty + p_{b,dyn}, \tag{5.10}$$

where $p_{a,dyn}$ and $p_{b,dyn}$ are the respective dynamic contributions to the pressure. Next, we consider the force balance at the apex of the drop surface (Fig. 1), that is the point where the z-axis pierces the drop surface:

$$\frac{2\sigma}{R_s} + \left(p_b - 2\eta_b \frac{\partial w_b}{\partial z}\right)_{ap} = \left(p_a - 2\eta_a \frac{\partial w_a}{\partial z}\right)_{ap}, \tag{5.11}$$

where the subscript 'ap' denotes that the expression in the parentheses should be estimated at the apex of the drop surface. Substituting p_a and p_b from Eq. (5.10) into Eq. (5.11), we get

$$\left(p_{b,dyn} - 2\eta_b \frac{\partial w_b}{\partial z}\right)_{ap} = \left(p_{a,dyn} - 2\eta_a \frac{\partial w_a}{\partial z}\right)_{ap}. \tag{5.12}$$

Further, in view of Eqs. (3.2), (3.3), and (5.11), we introduce dimensionless variables in Eq. (5.12):

$$\eta_b \left(\tilde{p}_b - 2\frac{\partial \tilde{w}_b}{\partial \tilde{z}}\right)_{ap} = \eta_a \left(\tilde{p}_a - 2\frac{\partial \tilde{w}_a}{\partial \tilde{z}}\right)_{ap}. \tag{5.13}$$

In the computations, it is convenient to express $\tilde{p}_a$ in the form:

$$\tilde{p}_a(\mathbf{r}) = \tilde{p}_{a,0}(\mathbf{r}) + \left(\tilde{p}_a - 2\frac{\partial \tilde{w}_a}{\partial \tilde{z}}\right)_{ap}, \tag{5.14}$$

where the last term in the parentheses is a constant (independent of $\mathbf{r}$). Equation (5.14) represents the definition of $\tilde{p}_{a,0}(\mathbf{r})$. At the apex of the drop surface, Eq. (5.14) gives the boundary condition for $\tilde{p}_{a,0}$:

$$\tilde{p}_{a,0}\big|_{ap} = 2\frac{\partial \tilde{w}_a}{\partial \tilde{z}}\bigg|_{ap}. \tag{5.15}$$

In view of Eqs. (5.9), (5.13), and (5.14), we obtain

$$f_a = f_{a,0} + \pi \left(\tilde{p}_a - 2\frac{\partial \tilde{w}_a}{\partial \tilde{z}}\right)_{ap} = f_{a,0} + \frac{\eta_b}{\eta_a}\pi \left(\tilde{p}_b - 2\frac{\partial \tilde{w}_b}{\partial \tilde{z}}\right)_{ap}, \tag{5.16}$$

where

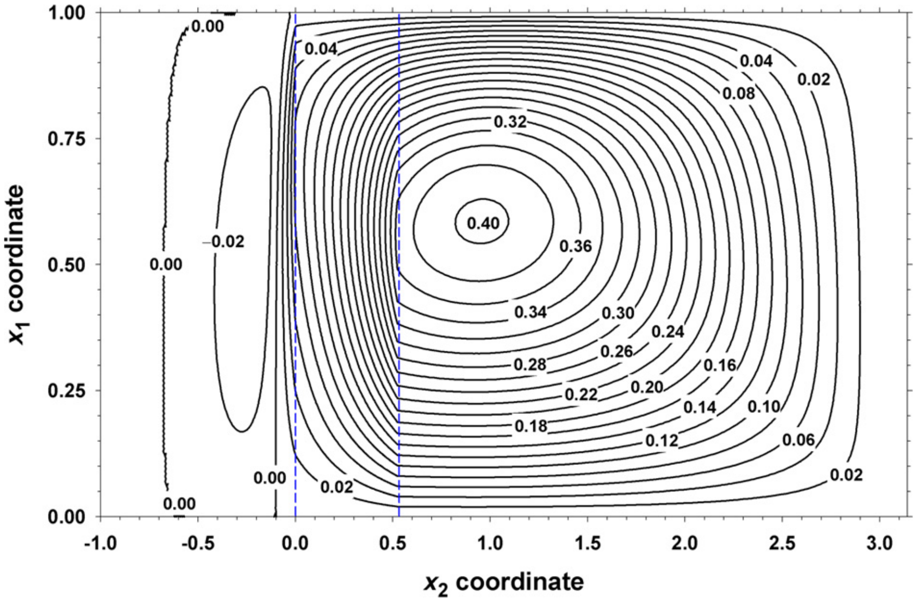

(a)

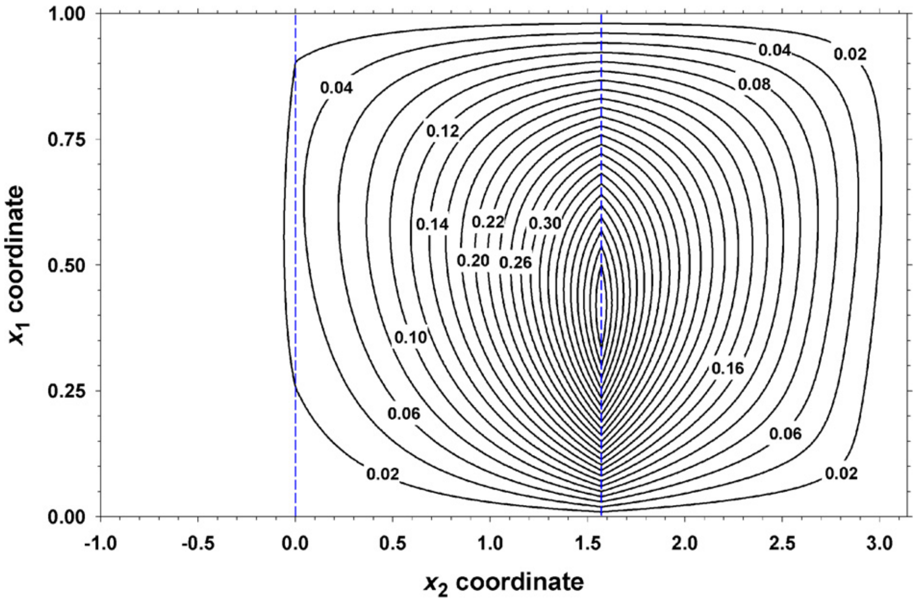

(b)

Fig. 5. Contour-plot diagrams of the dimensionless *radial* component of velocity, $\tilde{u}_\mathrm{f}(x_1, x_2)$, for different protrusion angles: (a) $\alpha = 30°$, (b) $\alpha = 90°$, (c) $\alpha = 150°$. The vertical dashed lines correspond to the boundaries between the domains A, B, and C in Fig. 3b.

$$f_{\mathrm{a},0} = 2\pi \int_0^1 \tilde{p}_{\mathrm{a},0} \tilde{r}\, d\tilde{r} \quad \text{at } z = 0. \tag{5.17}$$

Finally, in view of Eqs. (5.5) and (5.16), we can express the total hydrodynamic ejection force exerted on the drop in the following form:

$$F_\mathrm{h} = F_\mathrm{a} + F_\mathrm{b} = f_\mathrm{h} \eta_\mathrm{a} R_\mathrm{p} v_\mathrm{m}, \tag{5.18}$$

where

$$f_\mathrm{h} \equiv f_{\mathrm{a},0}(\alpha) + \frac{\eta_\mathrm{b}}{\eta_\mathrm{a}} \big[f_\mathrm{b}(\alpha) + f_\mathrm{ab}(\alpha) \big], \tag{5.19}$$

$$f_\mathrm{ab}(\alpha) = \pi \left(\tilde{p}_\mathrm{b} - 2 \frac{\partial \tilde{w}_\mathrm{b}}{\partial \tilde{z}} \right)_\mathrm{ap}. \tag{5.20}$$

Note, that because of the scaling procedure used in Section 3 the coefficients $f_{\mathrm{a},0}$, f_b, and f_ab depend only on the protrusion angle, α. Equation (5.19) shows that the total hydrodynamic coefficient, f_h, depends linearly on the ratio, $\eta_\mathrm{b}/\eta_\mathrm{a}$, of the dynamic viscosities of phases "b" and "a." Numerical results, as well as some approximate analytical expressions for $f_{\mathrm{a},0}(\alpha)$, $f_\mathrm{b}(\alpha)$, and $f_\mathrm{ab}(\alpha)$ are given in Section 5.2.

5.2. *Numerical results and discussion*

In the computations, it is convenient to express the coefficients $f_{\mathrm{a},0}$, f_b, and f_ab in terms of the obtained solution for the stream functions. After mathematical transformations given in Appendices D, E, and F in Supplementary material, we obtain

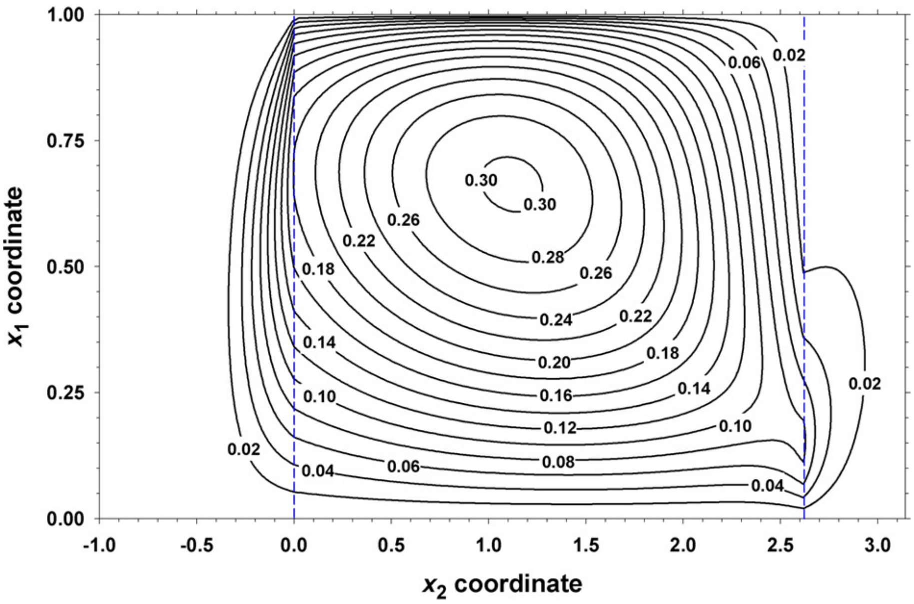

(c)

Fig. 5. *(continued)*

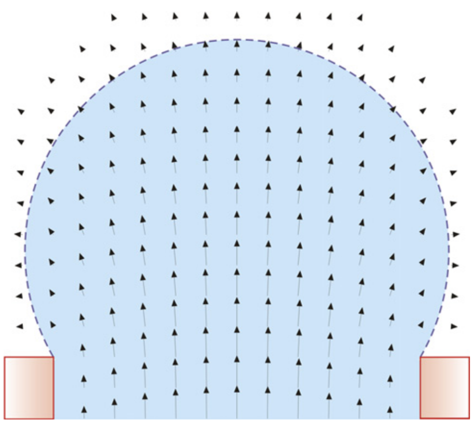

Fig. 6. Plot of the vectorial field of velocity for protrusion angle $\alpha = 120°$.

the following expressions for the three force coefficients:

$$f_{a,0} = c_1 + c_2 + c_3 + c_4, \qquad f_{ab} = c_5 - c_1, \tag{5.21}$$

$$f_b = 8\pi \int_0^1 \frac{x_1^2}{(1-x_1^2)^2} \frac{\partial^3 \psi_b}{\partial x_2^3} \, dx_1 \quad \text{at } x_2 = \pi, \tag{5.22}$$

where the coefficients c_j, $j = 1, \ldots, 5$, are defined as follows:

$$c_1 \equiv -2\pi \sin\alpha (1 + \cos\alpha), \tag{5.23}$$

$$c_2 \equiv -4\pi \frac{\partial^2 \psi_a}{\partial x_1 \partial x_2} \quad \text{at } x_1 = 0 \text{ and } x_2 = 0 - 0, \tag{5.24}$$

$$c_3 \equiv \frac{\pi}{3} \int_0^\alpha (1 + \cos x_2)^2 \frac{\partial^3 \psi_a}{\partial x_1^3} \, dx_2 + 4\pi \int_0^\alpha \sin x_2 (1 + \cos x_2) \frac{\partial^2 \psi_a}{\partial x_1 \partial x_2} \, dx_2 - 2\pi \int_0^\alpha \sin^2 x_2 \frac{\partial \psi_a}{\partial x_1} \, dx_2 \quad \text{at } x_1 = 0, \tag{5.25}$$

$$c_4 \equiv \pi \int_0^1 \left(\frac{\partial^3 \psi_a}{\partial x_2^3} + 6 \frac{\partial^2 \psi_a}{\partial x_2^2} + 6 \frac{\partial \psi_a}{\partial x_2} \right) (1 - x_1^2) \, dx_1 \quad \text{at } x_2 = 0 - 0, \tag{5.26}$$

$$c_5 \equiv \frac{\pi}{3} \int_\alpha^\pi (1 + \cos x_2)^2 \frac{\partial^3 \psi_b}{\partial x_1^3} \, dx_2 + 4\pi \int_\alpha^\pi \sin x_2 (1 + \cos x_2) \frac{\partial^2 \psi_b}{\partial x_1 \partial x_2} \, dx_2 - 2\pi \int_0^\alpha \sin^2 x_2 \frac{\partial \psi_a}{\partial x_1} \, dx_2 \quad \text{at } x_1 = 0. \tag{5.27}$$

It is important to note that the integrands in Eqs. (5.25)–(5.27) do not have any singular points and they can be calculated by using standard methods of numerical integration.

Knowing the values of stream functions, ψ_a and ψ_b, in the nodes of the numerical domains A, B, and C, we calculated their derivatives appearing in Eqs. (5.22), (5.24)–(5.27) by using their finite difference approximations of the second order [25,28–31]. Next, we calculated the integrals in Eqs. (5.22), (5.25)–(5.27) by means of the Simpson rule [29]. The latter has a higher precision than the finite difference approximation for the derivatives.

The calculated force coefficient $f_{a,0}(\alpha)$ is plotted in Fig. 7. As it could be anticipated from the velocity distributions (Figs. 4–6), $f_{a,0}(\alpha)$ has a maximum value at α close to 90°. The calculated maximal value of $f_{a,0}$ is equal to 19.66 and its position corresponds to $\alpha = 93.71°$. Further increase of the protrusion angle, α, leads to a decrease in $f_{a,0}$ followed by

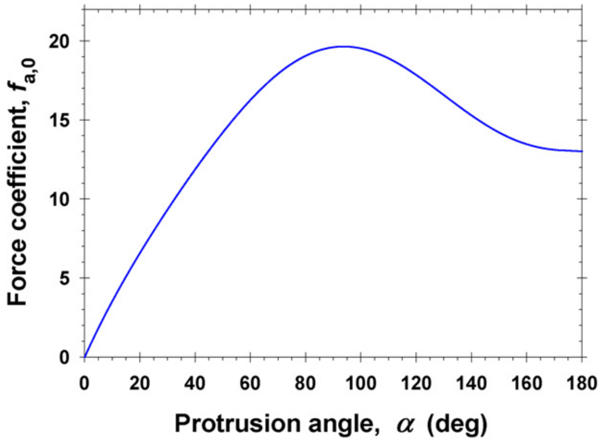

Fig. 7. Dependence of the hydrodynamic force coefficient $f_{a,0}$ on the protrusion angle α.

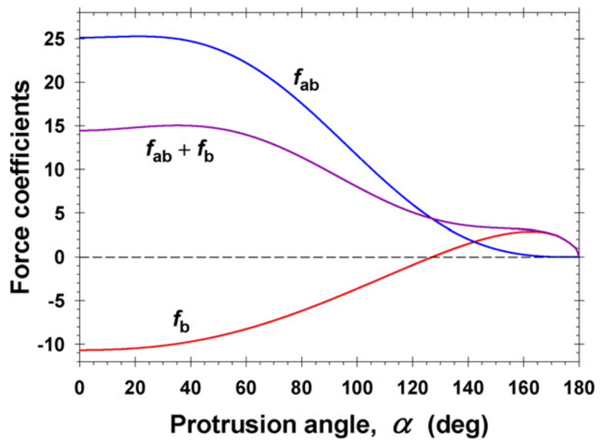

Fig. 8. Plots of the numerical results for the force coefficients f_{ab}, f_b, and their sum, vs the protrusion angle α.

a plateau at $\alpha \to 180°$. The latter plateau corresponds to the regime of free flow of liquid from a capillary. Our numerical calculations yielded $f_{a,0}(180°) = 13.04$. Analytical solution of this problem cannot be found [21], because the operator L^2 is not separable in the case of rotational symmetry. The value $f_{a,0}(180°) = 13.04$ (and the full dependence $f_{a,0}(\alpha)$) was not known before our computations.

The obtained numerical results for the force coefficients f_{ab} and f_b are shown in Fig. 8. The force coefficient f_{ab} is approximately constant for protrusion angles $\alpha < 40°$. A further increase of α leads to a fast decrease of f_{ab} to zero at $\alpha = 180°$. The force coefficient f_{ab} is positive for all values of α, which means that it favors the drop detachment. We recall that f_{ab} accounts for the jump of the hydrodynamic pressure across the drop surface at its apex. In contrast, the force coefficient f_b is negative for $0 \leqslant \alpha < 127°$, which means that f_b opposes the drop detachment from the pore (because of the hydrodynamic resistance of the outer liquid).

For $127° < \alpha < 180°$, f_b becomes positive and has a maximum value of 2.965 at $\alpha = 162°$; see Fig. 8. The positive values of f_b in this range of angles is due to the lifting action of the hydrodynamic resistance against the displacement of the outer liquid from the wedge-shaped zone between the drop surface and the flat horizontal solid surface around the opening of the pore (see Fig. 1). This lifting effect favors the drop detachment for $127° < \alpha < 180°$.

Note that in the total hydrodynamic force coefficient, f_h, the contributions of f_{ab} and f_b cannot be separated—they appear as a sum $f_{ab} + f_b$ in Eq. (5.19). Fig. 8 shows that $f_{ab} + f_b$ is positive for all values of the protrusion angle, α. In other words, the net effect of $f_{ab} + f_b$ favors the drop detachment. The limiting value of both f_{ab} and f_b for $\alpha \to 180°$ is zero (Fig. 8).

To find the exact limiting values of f_{ab} and f_b for $\alpha \to 0$, we obtained an analytical solution of the respective hydrodynamic problem (see Appendix G in Supplementary material). From this solution, we obtained $f_{ab}(0) = 8\pi \approx 25.13$ and $f_b(0) = -32/3 \approx -10.67$. Our independent numerical solution (Fig. 8) gives practically the same values, with a relative error that is smaller than 10^{-4}.

5.3. Approximate analytical expressions for the force coefficients

In the process of membrane emulsification (without applied cross flow), the radii of the detached drops are always greater than $2R_p$ [3]. This fact implies that the drop detachment occurs at protrusion angles $\alpha \geqslant 150°$. For easier calculation of the forces acting on the drop in this case, we obtained accurate analytical expressions for $f_{a,0}(\alpha)$, $f_{ab}(\alpha)$, and $f_b(\alpha)$, which are applicable in the interval $150° \leqslant \alpha \leqslant 180°$.

Interpolating our numerical results for $f_{a,0}(\alpha)$, we obtained

$$f_{a,0} \approx 15.4891 - 1.5710\cos(2\alpha) - 3.0621\cos^2(2\alpha) + 2.1847\cos^3(2\alpha), \tag{5.28}$$

which is applicable for $150° \leqslant \alpha \leqslant 180°$ with a relative error smaller than 10^{-3}. For the force coefficient, f_{ab}, we obtained the following interpolation formula:

$$f_{ab} \approx \frac{9}{2}\pi\xi\left(1 + \frac{1 - 433.64\xi}{12.063 + 9255.6\xi}\right), \tag{5.29}$$

$$\xi \equiv (1 + \cos\alpha)\sin\alpha. \tag{5.30}$$

Equations (5.29) and (5.30) are applicable for $150° \leqslant \alpha \leqslant 180°$ with a relative error smaller than 10^{-3}. Note that the first term in the right hand side of Eq. (5.29) corresponds to the combination of an expansion flow and a motion of a sphere in a viscous liquid [21], whereas the second term in the parenthesis is an interpolation correction, which accounts for the role of the solid surface (Fig. 1).

As mentioned above, for $\alpha > 127°$ the coefficient f_b is dominated by the hydrodynamic resistance against the displacement of the outer liquid from the region between the drop surface and the flat horizontal solid surface around the opening of the pore (see Fig. 1). For $\alpha \to \pi$, we could consider π–α as a small parameter, and we could use the lubrication approximation [21] to solve the hydrodynamic problem in this wedge-shape region. In Appendix H in Supplementary material, we have solved exactly this problem, in the framework of the lubrication approximation, and we have derived an analytical expression for the con-

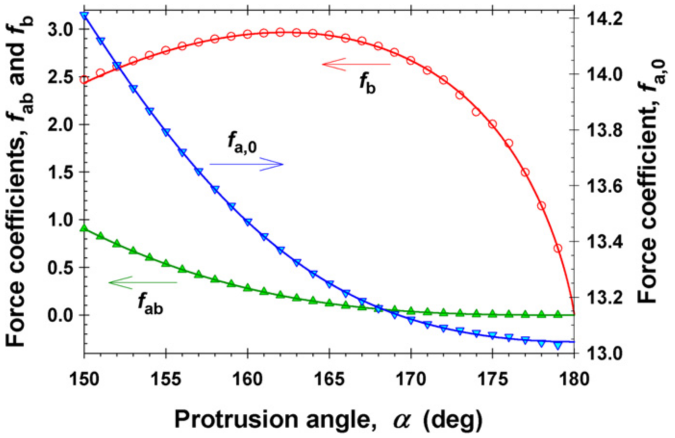

Fig. 9. Plot of the hydrodynamic force coefficients $f_{a,0}$, f_{ab}, and f_b vs the protrusion angle α. The symbols represent numerical results, whereas and lines are drawn using the interpolation formulas, Eqs. (5.28)–(5.32).

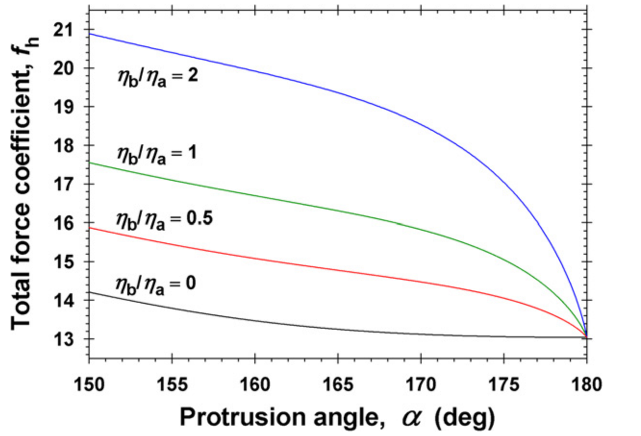

Fig. 10. Plot of the total hydrodynamic force coefficient, f_h, vs the protrusion angle, α, for four different values of the viscosity ratio, η_b/η_a.

tribution, f_{wedge}, of the wedge-shaped region to the force coefficient, f_b. The formula for f_{wedge} contains cosine integrals, and it is not so convenient for computations. More convenient is its series expansion:

$$f_{wedge} \approx 6\pi \cot\left(\frac{\alpha}{2}\right)\left[0.79381 - \ln(\pi-\alpha) + \frac{(\pi-\alpha)^2}{24} - \frac{(\pi-\alpha)^4}{1440}\right], \tag{5.31}$$

which is applicable for $150° \leqslant \alpha \leqslant 180°$ with a relative error smaller than 10^{-7}. In other words, Eq. (5.31) is practically the exact solution of the problem in lubrication approximation. To obtain f_b we added to f_{wedge} the effect of the flow around the apex of the drop. To quantify the latter effect, we scaled the contribution of the flow around the apex with the half of the Stokes friction coefficient, and fitted the numerical results. The final interpolation formula for f_b reads:

$$f_b = f_{wedge} - 3\pi \cot\left(\frac{\alpha}{2}\right)\left\{1 + 0.94095 \times \left[1 - \exp\left(-25.822\cot\frac{\alpha}{2}\right)\right]\right\}. \tag{5.32}$$

Equation (5.32) has a relative error smaller than 10^{-3} for $150° \leqslant \alpha \leqslant 180°$.

Fig. 9 illustrates the accuracy of the approximate analytical expressions, Eqs. (5.28)–(5.32). The symbols in the figure correspond to the numerical results, whereas the solid lines are drawn in accordance with Eqs. (5.28)–(5.32). The plot confirms the excellent accuracy of the interpolation formulas.

5.4. The total hydrodynamic force coefficient, f_h

Equation (5.18) for the total hydrodynamic ejection force, F_h, can be represented in the form:

$$\frac{F_h}{R_p v_m} \equiv \eta_a f_h = \eta_a f_{a,0}(\alpha) + \eta_b\left[f_{ab}(\alpha) + f_b(\alpha)\right]. \tag{5.33}$$

We recall that $f_{a,0}(\alpha)$, $f_{ab}(\alpha)$ and $f_b(\alpha)$ are universal functions of α, which are independent of the viscosities of the two liquid phases: η_a and η_b. As seen in Figs. 7 and 8, for $\alpha \to 0$ we have $f_{a,0} \to 0$, whereas $f_{ab} + f_b \to 14.45$. Hence, for small α the hydrodynamic force is sensitive to the viscosity of the outer phase, η_b, and insensitive to the viscosity of the inner phase, η_a; see Eq. (5.33).

In contrast, for $\alpha \to 180°$ we have $f_{a,0} \to 13.04$, whereas $f_{ab} + f_b \to 0$. Hence, for large α the hydrodynamic force is sensitive to the viscosity of the inner phase, η_a, and not so sensitive to the viscosity of the outer phase, η_b; see Eq. (5.33).

To illustrate the effect of the total hydrodynamic force on the viscosities of the two phases, in Fig. 10 we have plotted the hydrodynamic force coefficient $f_h(\alpha)$ for $150° \leqslant \alpha \leqslant 180°$ and for four different values of the viscosity ratio, η_a/η_b. The curves in Fig. 10 are calculated by means of Eq. (5.19), along with Eqs. (5.28)–(5.32). As mentioned above, the interval $150° \leqslant \alpha \leqslant 180°$ corresponds to the region where the drops detach from the pore in the process of membrane emulsification. Fig. 10 indicates that f_h noticeably increases with the rise of η_b/η_a. Hence, at fixed η_a, the increase of the viscosity of the outer phase, η_b, will favor the drop detachment from the pore. The latter effect is due to the lifting action of the hydrodynamic resistance against the displacement of the outer liquid from the wedge-shaped region between the drop surface and the flat horizontal solid surface around the opening of the pore; see Fig. 1 and Eq. (5.31).

Finally, because $f_{a,0}$ and $f_{ab} + f_b$ are nonnegative (Figs. 7 and 8), the increase of both η_a and η_b increases the total hydrodynamic ejection force, F_h, see Eq. (5.33). The calculation of F_h is a necessary condition for prediction of the size of the detached drops. In the second part of this study [33], a theoretical model is proposed, which assumes that at the moment of breakup, the hydrodynamic ejection force acting on the drop is equal to the critical capillary force that corresponds to the stability–instability transition in the drop shape. In its own turn, the capillary force is related to the effects of interfacial tension and surfactant adsorption. A comparison of the full theory with experimental data could be found in Ref. [33].

6. Summary and conclusions

Our aim in the present study is to calculate the hydrodynamic ejection force acting on a microscopic emulsion drop, which is continuously growing at a capillary tip (Fig. 1). This force could cause drop detachment in the process of membrane and microchannel emulsification, and affects the size of the released drops. Such microscopic drops are not deformed by gravity and their formation happens at small Reynolds numbers despite the fact that the typical period of drop generation is of the order of 0.1 s.

First, we calculated the distribution of the velocity field inside the capillary, within the growing droplet and in the outer liquid phase. For this goal, we introduced appropriate curvilinear coordinates, which transform the inner and outer integration domains into rectangles (Fig. 3). The hydrodynamic problem is reduced to a single partial differential equation for the stream function; see Eqs. (3.8), (4.11), and (4.12). The respective boundary conditions are represented in terms of the curvilinear coordinates (Section 4.2). The boundary problem is solved numerically and the spatial distributions of the stream function and the velocity components are calculated (Figs. 4–6).

Second, we calculated the hydrodynamic force acting on the drop. The problem is reduced to the determination of three universal functions of the protrusion angle, α, viz. $f_{\mathrm{a},0}(\alpha)$, $f_{\mathrm{ab}}(\alpha)$, and $f_{\mathrm{b}}(\alpha)$; see Eqs. (5.18)–(5.22). The latter functions are independent of the pore size, of the viscosities of the two liquids, and of the characteristic rate of the process. These universal functions were computed numerically and plotted in Figs. 7 and 8. In addition, for their easier calculation, simple interpolation formulas are obtained; see Eqs. (5.28)–(5.32) and Fig. 9. It turns out that the increase in the viscosity of each of the two liquid phases increases the total hydrodynamic force, F_{h}, and its tendency to detach the drop from the tip of the capillary; see Eq. (5.33) and Fig. 10.

The results of the present paper are utilized in the second part of this study [33], where a physical condition for drop detachment from the pore is formulated; the size of the detached drops is calculated under the alternative conditions of constant pressure and constant flow rate and, finally, the theory is applied to interpret experimental size distributions of drops obtained by membrane emulsification.

Acknowledgments

This work was supported in part by the EC Inco-Copernicus Project, No. IC15CT980911, and in part by the program "Cooperation and Networking for Excellence" (CONEX), Project "Emulsions with Nanoparticles for New Materials" (EMMA), financed by the Austrian Ministry of Education, Science and Culture.

Supplementary material

The online version of this article contains additional supplementary material, which consists of Appendices A–H.

Please visit DOI: 10.1016/j.jcis.2007.08.061.

References

[1] V. Schröder, H. Schubert, Colloids Surf. A 152 (1999) 103–109.
[2] S.M. Joscelyne, G. Trägårdh, J. Membrane Sci. 169 (2000) 107–117.
[3] N.C. Christov, D.N. Ganchev, N.D. Vassileva, N.D. Denkov, K.D. Danov, P.A. Kralchevsky, Colloids Surf. A 209 (2002) 83–104.
[4] C. Charcosset, I. Limayem, H. Fessi, J. Chem. Technol. Biotechnol. 79 (2004) 209–218.
[5] G.T. Vladislavljević, R.A. Williams, Adv. Colloid Interface Sci 113 (2005) 1–20.
[6] T. Kawakatsu, Y. Kikuchi, M. Nakajima, J. Am. Oil Chem. Soc. 74 (1997) 317–321.
[7] T. Kawakatsu, H. Komori, M. Nakajima, Y. Kikuchi, T. Yonemoto, J. Chem. Eng. Jpn. 32 (1999) 241–244.
[8] S. Sugiura, M. Nakajima, M. Seki, Langmuir 18 (2002) 5708–5712.
[9] S. Sugiura, M. Nakajima, M. Seki, Langmuir 18 (2002) 3854–3859.
[10] M. Rayner, G. Trägårdh, C. Trägårdh, P. Dejmek, J. Colloid Interface Sci. 279 (2004) 175–185.
[11] M. Rayner, G. Trägårdh, C. Trägårdh, Colloids Surf. A 266 (2005) 1–17.
[12] I. Kobayashi, S. Mukataka, M. Nakajima, Langmuir 20 (2004) 9868–9877.
[13] I. Kobayashi, S. Mukataka, M. Nakajima, Langmuir 21 (2005) 5722–5730.
[14] S. van der Graaf, T. Nisisako, C.G.P.H. Schroën, R.G.M. van der Sman, R.M. Boom, Langmuir 22 (2006) 4144–4152.
[15] V. Schröder, O. Behrend, H. Schubert, J. Colloid Interface Sci. 202 (1998) 334–340.
[16] L.D. Landau, E.M. Lifshitz, Fluid Mechanics, Pergamon Press, Oxford, 1984.
[17] G.K. Batchelor, An Introduction to Fluid Dynamics, Cambridge Univ. Press, Cambridge, 1967.
[18] D.A. Edwards, H. Brenner, D.T. Wasan, Interfacial Transport Processes and Rheology, Butterworth–Heinemann, Boston, 1991.
[19] J.C. Slattery, Interfacial Transport Phenomena, Springer-Verlag, New York, 1990.
[20] J. Happel, H. Brenner, Low Reynolds Number Hydrodynamics with Special Applications to Particular Media, Prentice Hall, Englewood Cliffs, NJ, 1965.
[21] L.G. Leal, Laminar Flow and Convective Transport Processes: Scaling Principles and Asymptotic Analysis, Butterworth–Heinemann, MA, 1992.
[22] V. Levich, Physicochemical Hydrodynamics, Prentice Hall, Englewood Cliffs, NJ, 1962.
[23] I.B. Ivanov (Ed.), Thin Liquid Films, Dekker, New York, 1988.
[24] K.D. Danov, J. Colloid Interface Sci. 235 (2001) 144–149.
[25] G.A. Korn, T.M. Korn, Mathematical Handbook, McGraw–Hill, New York, 1968.
[26] G. Arfken, Mathematical Methods for Physicists, Academic Press, Orlando, FL, 1970.
[27] P. Moon, D.E. Spencer, Field Theory Handbook, Including Coordinate Systems, Differential Equations, and Their Solutions, Springer-Verlag, New York, 1988.
[28] M. Abramowitz, I.A. Stegun, Handbook of Mathematical Functions, National Bureau of Standards, Washington, DC, 1984.
[29] W.H. Press, B.P. Flannery, S.A. Teukolsky, W.T. Vetterling, Numerical Recipes in FORTRAN: The Art of Scientific Computing, Cambridge Univ. Press, New York, 1992.
[30] C.A.J. Fletcher, Computational Techniques for Fluid Dynamics. 1. Fundamental and General Techniques, Springer-Verlag, New York, 1991.
[31] C.A.J. Fletcher, Computational Techniques for Fluid Dynamics. 2. Specific Techniques for Different Flow Categories, Springer-Verlag, New York, 1991.
[32] D. Möbius, R. Miller (Eds.), Drops and Bubbles in Interfacial Research, Elsevier, Amsterdam, 1998.
[33] N.C. Christov, K.D. Danov, D.K. Danova, P.A. Kralchevsky, Langmuir, in press.

Supplementary Material

For the article

Hydrodynamic forces acting on a microscopic emulsion drop growing at a capillary tip in relation to the process of membrane emulsification

Authors: Krassimir D. Danov, Darina K. Danova, Peter A. Kralchevsky

Laboratory of Chemical Physics & Engineering, Faculty of Chemistry, University of Sofia, 1164 Sofia, Bulgaria

(Journal of Colloid and Interface Science)

Here, we have used numbers of sections, equations and figures, which are the same as in the main text of the article. The list of references cited in the present material is given at its end.

Appendix A. Derivation of the boundary conditions (3.14) and (3.15)

From Eqs. (2.13) and (3.7), we express the normal component of velocity at the drop surface:

$$\mathbf{n}\cdot\tilde{\mathbf{v}}_{\mathrm{f}} = \sin\theta\frac{\partial\psi_{\mathrm{f}}}{\partial\tilde{z}} - \cos\theta\frac{\partial\psi_{\mathrm{f}}}{\partial\tilde{r}} - \frac{\cos\theta}{\tilde{r}}\psi_{\mathrm{f}}\,, \tag{A.1}$$

where f = a, b. Equation (A.1) can be simplified with the help of spherical coordinates connected to the drop center, O_{s}, with dimensionless coordinates $(\tilde{r}_{\mathrm{sph}},\theta)$:

$$\tilde{r} = \tilde{r}_{\mathrm{sph}}\sin\theta\,,\ \tilde{z} = \tilde{z}_{\mathrm{d}} + \tilde{r}_{\mathrm{sph}}\cos\theta\,. \tag{A.2}$$

Thus, Eq. (A.1) reduces to:

$$\mathbf{n}\cdot\tilde{\mathbf{v}}_{\mathrm{f}} = -\frac{1}{\tilde{r}_{\mathrm{sph}}\sin\theta}\frac{\partial}{\partial\theta}(\psi_{\mathrm{f}}\sin\theta)\,. \tag{A.3}$$

In view of Eq. (3.2), the dimensionless spherical coordinate at the drop surface is equal to $\tilde{r}_{\mathrm{sph}} = 1/\sin\alpha$. Using the expression for the normal velocity component at the drop surface, Eq. (2.12), we bring Eq. (A.3) in the form:

$$\frac{\partial}{\partial\theta}(\psi_{\mathrm{f}}\sin\theta) = -\frac{1+\cos\alpha}{1-\cos\alpha}(\cos\theta-\cos\alpha)\frac{\sin\theta}{\sin\alpha}\,. \tag{A.4}$$

Further, we integrate Eq. (A.4) from 0 to θ to obtain:

$$\psi_{\mathrm{f}} \sin\theta = \frac{1}{\sin\alpha}\frac{1+\cos\alpha}{1-\cos\alpha}[\frac{\cos^2\theta - 1}{2} - \cos\alpha(\cos\theta - 1)]\,. \tag{A.5}$$

After mathematical transformations, Eq. (A.5) acquires the form:

$$\psi_{\mathrm{f}} = \frac{(1+\cos\alpha)\sin\theta}{(1-\cos\alpha)\sin\alpha}(\frac{\cos\alpha}{1+\cos\theta} - \frac{1}{2})\,, \tag{A.6}$$

which is identical to Eq. (3.14). It is important to note that the stream function in Eq. (A.6) is continuous at the edge of the pore, i.e. the value of ψ_{f} is equal to $-1/2$ at $\theta = \alpha$, see also Eqs. (3.12) and (3.13). With the help of Eqs. (2.13) and (3.7), we calculate the tangential component of velocity at the drop surface:

$$\mathbf{t}\cdot\tilde{\mathbf{v}}_{\mathrm{f}} = \cos\theta\frac{\partial\psi_{\mathrm{f}}}{\partial\tilde{z}} + \sin\theta\frac{\partial\psi_{\mathrm{f}}}{\partial\tilde{r}} + \frac{\sin\theta}{\tilde{r}}\psi_{\mathrm{f}}\,, \tag{A.7}$$

where f = a, b. At the drop surface, $\tilde{r} = (R_{\mathrm{s}}\sin\theta)/R_{\mathrm{p}}$, and then Eq. (A.7) reduces to:

$$\mathbf{t}\cdot\tilde{\mathbf{v}}_{\mathrm{f}} = \sin\theta\frac{\partial\psi_{\mathrm{f}}}{\partial\tilde{r}} + \cos\theta\frac{\partial\psi_{\mathrm{f}}}{\partial\tilde{z}} + \psi_{\mathrm{f}}\sin\alpha\,. \tag{A.8}$$

The sum of the partial derivatives in Eq. (A.8) is equal to the directional (normal) derivative of the stream function at the drop surface:

$$\frac{\partial\psi_{\mathrm{f}}}{\partial n} = \mathbf{n}\cdot\nabla\psi_{\mathrm{f}} = \sin\theta\frac{\partial\psi_{\mathrm{f}}}{\partial\tilde{r}} + \cos\theta\frac{\partial\psi_{\mathrm{f}}}{\partial\tilde{z}}\,. \tag{A.9}$$

which coincides with Eq. (3.15).

Appendix B. Derivation of the boundary conditions (4.17)–(4.19)

In view of Eq. (A.2), the radial and vertical coordinates at the drop surface are related to the polar angle, θ, as follows:

$$\tilde{r} = \frac{\sin\theta}{\sin\alpha}\,,\ \tilde{z} = \frac{\cos\theta - \cos\alpha}{\sin\alpha}\,. \tag{B.1}$$

Substituting $\tilde{z}$ from Eq. (4.3) into Eq. (B.1), and having in mind that $x_2 = \alpha$ at the drop surface, we derive an expression for $\cos\theta$:

$$\cos\theta = \frac{1-x_1^2}{1+x_1^2+(1-x_1^2)\cos\alpha}\sin^2\alpha + \cos\alpha = \frac{1-x_1^2+(1+x_1^2)\cos\alpha}{1+x_1^2+(1-x_1^2)\cos\alpha}\,. \tag{B.2}$$

With the help of Eqs. (3.14), (B.1) and (4.3), the stream function at the drop surface can be presented in the form:

$$\psi_a = \psi_b = \frac{(1+\cos\alpha)x_1}{(1-\cos\alpha)h}\left(\frac{2\cos\alpha}{1+\cos\theta}-1\right) \text{ at } x_2 = \alpha. \tag{B.3}$$

Next, substituting $\cos\theta$ from Eq. (B.2) into Eq. (B.3), one derives:

$$\psi_a = \psi_b = \frac{1}{1-\cos\alpha}\frac{x_1}{h}(h\cos\alpha - 1 - \cos\alpha) \text{ at } x_2 = \alpha. \tag{B.4}$$

At the drop surface, Eq. (4.4) acquires the form:

$$h = 1 + x_1^2 + (1-x_1^2)\cos\alpha \text{ at } x_2 = \alpha. \tag{B.5}$$

Substituting Eq. (B.5) into Eq. (B.4), we get:

$$\psi_a = \psi_b = -x_1 \frac{1+(1-x_1^2)\cos\alpha}{1+x_1^2+(1-x_1^2)\cos\alpha} \text{ at } x_2 = \alpha, \tag{B.6}$$

which is equivalent to Eq. (4.17). Further, with the help of Eq. (4.8), we express the directional derivative in the form [1,2]:

$$\frac{\partial\psi_f}{\partial n} = \frac{1}{h_2}\frac{\partial\psi_f}{\partial x_2} = \frac{h}{1-x_1^2}\frac{\partial\psi_f}{\partial x_2} \text{ at } x_2 = \alpha \text{ and f = a, b.} \tag{B.7}$$

The substitution of Eq. (B.5) into Eq. (B7) yields:

$$\frac{\partial\psi_f}{\partial n} = \left(\frac{1+x_1^2}{1-x_1^2} + \cos\alpha\right)\frac{\partial\psi_f}{\partial x_2} \text{ at } x_2 = \alpha \text{ and f = a, b.} \tag{B.8}$$

With the help of Eqs. (4.3) and (B.8), we bring the boundary condition, Eq. (3.15), in the form:

$$\left(\frac{1+x_1^2}{1-x_1^2} + \cos\alpha\right)\frac{\partial\psi_f}{\partial x_2} + \psi_f \sin\alpha = 0 \text{ at } x_2 = \alpha \text{ and f = a, b,} \tag{B.9}$$

which is equivalent to Eq. (4.18). Furthermore, the projection $\mathbf{e}_2 \cdot \mathbf{v}_f$ (Fig. 3a) is calculated from the following general relationship [1,2]:

$$\mathbf{e}_2 \cdot \mathbf{v}_f = \frac{1}{h_2}\frac{\partial\tilde{r}}{\partial x_2}\tilde{u}_f + \frac{1}{h_2}\frac{\partial\tilde{z}}{\partial x_2}\tilde{w}_f \text{ (f = a ,b).} \tag{B.10}$$

Substituting the radial and vertical velocity components from Eq. (3.7) into Eq. (B.10), we obtain:

$$\mathbf{e}_2 \cdot \mathbf{v}_f = \frac{1}{h_2}\frac{\partial\tilde{r}}{\partial x_2}\frac{\partial\psi_f}{\partial\tilde{z}} - \frac{1}{h_2}\frac{\partial\tilde{z}}{\partial x_2}\left(\frac{\partial\psi_f}{\partial\tilde{r}} + \frac{\psi_f}{\tilde{r}}\right) \text{ (f = a ,b).} \tag{B.11}$$

With the help of Eqs. (4.6) and (4.7), we transform the right-hand side of Eq. (B.11):

$$\mathbf{e}_2 \cdot \mathbf{v}_f = -\frac{1-x_1^2}{2h_2}\left(\frac{\partial\tilde{r}}{\partial x_1}\frac{\partial\psi_f}{\partial\tilde{r}} + \frac{\partial\tilde{z}}{\partial x_1}\frac{\partial\psi_f}{\partial\tilde{z}} + \frac{\partial\tilde{r}}{\partial x_1}\frac{\psi_f}{\tilde{r}}\right) \text{ (f = a ,b).} \tag{B.12}$$

Next, from Eq. (4.8) and (B.12) we derive:

$$\mathbf{e}_2 \cdot \mathbf{v}_\mathrm{f} = -\frac{1}{h_1}\left(\frac{\partial \psi_\mathrm{f}}{\partial x_1} + \frac{\partial \tilde{r}}{\partial x_1}\frac{\psi_\mathrm{f}}{\tilde{r}}\right) \text{ (f = a ,b).} \tag{B.13}$$

The circumference ($\tilde{r} = 1$, $\tilde{z} = 0$), which represents the edge at the orifice of the pore, corresponds to the coordinate line $x_1 = 1$. From Eqs. (4.3), (4.4) and (4.8) it follows:

$$h = 2,\ h_1 = 1,\ \frac{\partial \tilde{r}}{\partial x_1} = \cos x_2 \text{ at } x_1 = 1. \tag{B.14}$$

Therefore, from Eqs. (B.13) and (B.14) the non-slip boundary condition, $\mathbf{v}_\mathrm{f} = \mathbf{0}$ at the edge reads:

$$\frac{\partial \psi_\mathrm{f}}{\partial x_1} = -\psi_\mathrm{f} \cos x_2 = \frac{\cos x_2}{2} \text{ at } x_1 = 1,\ 0 \le x_2 \le \pi, \text{ and f = a ,b;} \tag{B.15}$$

see Eq. (4.19).

Appendix C. Derivation of the boundary conditions (4.22)–(4.24)

With the help of Eq. (4.2), we express the derivatives in Eq. (4.20) for the domain A:

$$\frac{\partial \psi_\mathrm{a}}{\partial \tilde{z}} = (1+x_2)^2 \frac{\partial \psi_\mathrm{a}}{\partial x_2}, \tag{C.1}$$

$$\frac{\partial^2 \psi_\mathrm{a}}{\partial \tilde{z}^2} = (1+x_2)^2 \frac{\partial}{\partial x_2}\left[(1+x_2)^2 \frac{\partial \psi_\mathrm{a}}{\partial x_2}\right] = (1+x_2)^4 \frac{\partial^2 \psi_\mathrm{a}}{\partial x_2^2} + 2(1+x_2)^3 \frac{\partial \psi_\mathrm{a}}{\partial x_2}, \tag{C.2}$$

$$\frac{\partial^3 \psi_\mathrm{a}}{\partial \tilde{z}^3} = (1+x_2)^2 \frac{\partial}{\partial x_2}\left[(1+x_2)^4 \frac{\partial^2 \psi_\mathrm{a}}{\partial x_2^2} + 2(1+x_2)^3 \frac{\partial \psi_\mathrm{a}}{\partial x_2}\right] =$$

$$= (1+x_2)^6 \frac{\partial^3 \psi_\mathrm{a}}{\partial x_2^3} + 6(1+x_2)^5 \frac{\partial^2 \psi_\mathrm{a}}{\partial x_2^2} + 6(1+x_2)^4 \frac{\partial \psi_\mathrm{a}}{\partial x_2}. \tag{C.3}$$

From Eqs. (C.1)–(C.3), we obtain the values of the derivatives at the boundary $\tilde{z} = 0$, which corresponds to $x_2 = 0$:

$$\frac{\partial \psi_\mathrm{a}}{\partial \tilde{z}} = \frac{\partial \psi_\mathrm{a}}{\partial x_2}, \quad \frac{\partial^2 \psi_\mathrm{a}}{\partial \tilde{z}^2} = \frac{\partial^2 \psi_\mathrm{a}}{\partial x_2^2} + 2\frac{\partial \psi_\mathrm{a}}{\partial x_2}, \quad \frac{\partial^3 \psi_\mathrm{a}}{\partial \tilde{z}^3} = \frac{\partial^3 \psi_\mathrm{a}}{\partial x_2^3} + 6\frac{\partial^2 \psi_\mathrm{a}}{\partial x_2^2} + 6\frac{\partial \psi_\mathrm{a}}{\partial x_2}. \tag{C.4}$$

With the help of Eq. (4.10), we calculate the first and second z-derivatives in the domain B:

$$\frac{\partial \psi_\mathrm{a}}{\partial \tilde{z}} = -x_1 \sin x_2 \frac{\partial \psi_\mathrm{a}}{\partial x_1} + \left(1 + \frac{1+x_1^2}{1-x_1^2}\cos x_2\right)\frac{\partial \psi_\mathrm{a}}{\partial x_2}, \tag{C.5}$$

$$\frac{\partial^2\psi_a}{\partial \tilde{z}^2} = -x_1 \sin x_2 \frac{\partial}{\partial x_1}[-x_1 \sin x_2 \frac{\partial \psi_a}{\partial x_1} + (1+\frac{1+x_1^2}{1-x_1^2}\cos x_2)\frac{\partial \psi_a}{\partial x_2}] +$$

$$+ (1+\frac{1+x_1^2}{1-x_1^2}\cos x_2)\frac{\partial}{\partial x_2}[-x_1 \sin x_2 \frac{\partial \psi_a}{\partial x_1} + (1+\frac{1+x_1^2}{1-x_1^2}\cos x_2)\frac{\partial \psi_a}{\partial x_2}] . \qquad \text{(C.6)}$$

After some mathematical transformations, Eq. (C.6) reduces to:

$$\frac{\partial^2\psi_a}{\partial \tilde{z}^2} = -x_1 \sin x_2 [-\sin x_2 \frac{\partial}{\partial x_1}(x_1 \frac{\partial \psi_a}{\partial x_1}) + 2(1+\frac{1+x_1^2}{1-x_1^2}\cos x_2)\frac{\partial^2 \psi_a}{\partial x_1 \partial x_2} + \frac{4x_1 \cos x_2}{(1-x_1^2)^2}\frac{\partial \psi_a}{\partial x_2}] +$$

$$+ (1+\frac{1+x_1^2}{1-x_1^2}\cos x_2)[-x_1 \cos x_2 \frac{\partial \psi_a}{\partial x_1} + (1+\frac{1+x_1^2}{1-x_1^2}\cos x_2)\frac{\partial^2 \psi_a}{\partial x_2^2} - \frac{1+x_1^2}{1-x_1^2}\sin x_2 \frac{\partial \psi_a}{\partial x_2}] . \qquad \text{(C.7)}$$

At the boundary $x_2 = 0$, Eqs. (C.5) and (C.7) yield:

$$\frac{\partial \psi_a}{\partial \tilde{z}} = \frac{2}{1-x_1^2}\frac{\partial \psi_a}{\partial x_2} , \quad \frac{\partial^2 \psi_a}{\partial \tilde{z}^2} = \frac{4}{(1-x_1^2)^2}\frac{\partial^2 \psi_a}{\partial x_2^2} - \frac{2x_1}{1-x_1^2}\frac{\partial \psi_a}{\partial x_1} , \qquad \text{(C.8)}$$

which, in view of Eq. (C.4), are equivalent to Eqs. (4.22) and (4.23). Further, by differentiation of Eq. (C.5) one obtains the third z-derivative at the boundary $x_2 = 0$:

$$\frac{\partial^3 \psi_a}{\partial \tilde{z}^3} = \frac{2}{1-x_1^2}\frac{\partial}{\partial x_2}(\frac{\partial^2 \psi_a}{\partial \tilde{z}^2}) . \qquad \text{(C.9)}$$

Substituting Eq. (C.7) into Eq. (C.9) and setting $x_2 = 0$, we derive:

$$\frac{\partial^3 \psi_a}{\partial \tilde{z}^3} = \frac{8}{(1-x_1^2)^3}\frac{\partial^3 \psi_a}{\partial x_2^3} - \frac{12x_1}{(1-x_1^2)^2}\frac{\partial^2 \psi_a}{\partial x_1 \partial x_2} - \frac{4(1+3x_1^2)}{(1-x_1^2)^3}\frac{\partial \psi_a}{\partial x_2} \text{ at } x_2 = 0. \qquad \text{(C.10)}$$

Combining Eqs. (C.4) and (C.10), one obtains Eq. (4.24).

Appendix D. Expression for the force coefficient $f_{a,0}$

To obtain a convenient expression for numerical calculation of the force coefficient $f_{a,0}$, we represent the integral in Eq. (5.17) as follows:

$$f_{a,0} = 2\pi \int_0^1 [\tilde{p}_{a,0}\tilde{r} - \frac{\partial}{\partial \tilde{r}}(\tilde{r}\tilde{u}_a)] d\tilde{r} = \pi \int_0^1 [\tilde{p}_{a,0} - \frac{1}{\tilde{r}}\frac{\partial}{\partial \tilde{r}}(\tilde{r}\tilde{u}_a)] d(\tilde{r}^2 - 1) \text{ at } z = 0. \qquad \text{(D.1)}$$

Integrating Eq. (D.1) by parts, one derives:

$$f_{a,0} = \pi[\tilde{p}_{a,0} - \frac{1}{\tilde{r}}\frac{\partial}{\partial \tilde{r}}(\tilde{r}\tilde{u}_a)]_O - \pi \int_0^1 (\tilde{r}^2 - 1)\frac{\partial}{\partial \tilde{r}}[\tilde{p}_{a,0} - \frac{1}{\tilde{r}}\frac{\partial}{\partial \tilde{r}}(\tilde{r}\tilde{u}_a)] d\tilde{r} \text{ at } z = 0, \qquad \text{(D.2)}$$

where the subscript "O" denotes the respective value calculated at the origin of the cylindrical coordinate system. Eq. (D.2) can be simplified by means of the Stokes equations, Eqs. (3.4) and (3.5):

$$f_{\mathrm{a},0} = \pi(\tilde{p}_{\mathrm{a},0} + \frac{\partial \tilde{w}_{\mathrm{a}}}{\partial \tilde{z}})_O - \pi\int_0^1 (\tilde{r}^2 - 1)\frac{\partial^2 \tilde{u}_{\mathrm{a}}}{\partial \tilde{z}^2}\,\mathrm{d}\tilde{r} \quad \text{at } z = 0. \tag{D.3}$$

Integrating the Stokes equation (3.6) with respect to the vertical coordinate, z, from 0 to the apex of the drop, one obtains the following relationship at the axis of symmetry:

$$(\tilde{p}_{\mathrm{a},0} - \frac{\partial \tilde{w}_{\mathrm{a}}}{\partial \tilde{z}})_{\mathrm{ap}} - (\tilde{p}_{\mathrm{a},0} - \frac{\partial \tilde{w}_{\mathrm{a}}}{\partial \tilde{z}})_O = \int_0^{\tilde{z}_{\mathrm{ap}}} \frac{1}{\tilde{r}}\frac{\partial}{\partial \tilde{r}}(\tilde{r}\frac{\partial \tilde{w}_{\mathrm{a}}}{\partial \tilde{r}})\,\mathrm{d}\tilde{z} \quad \text{at } r = 0, \tag{D.4}$$

where $\tilde{z}_{\mathrm{ap}}$ is the dimensionless vertical coordinate of the drop apex. Using Eqs. (5.15) and (D.4), we determine the pressure at the origin of the cylindrical coordinate system:

$$(\tilde{p}_{\mathrm{a},0})_O = (\frac{\partial \tilde{w}_{\mathrm{a}}}{\partial \tilde{z}})_{\mathrm{ap}} + (\frac{\partial \tilde{w}_{\mathrm{a}}}{\partial \tilde{z}})_O - \int_0^{\tilde{z}_{\mathrm{ap}}} \frac{1}{\tilde{r}}\frac{\partial}{\partial \tilde{r}}(\tilde{r}\frac{\partial \tilde{w}_{\mathrm{a}}}{\partial \tilde{r}})\,\mathrm{d}\tilde{z} \quad \text{at } r = 0. \tag{D.5}$$

Substituting Eq. (D.5) into Eq. (D.3), we obtain:

$$f_{\mathrm{a},0} = c_1 + c_2 + c_3 + c_4\,, \tag{D.6}$$

where

$$c_1 \equiv \pi(\frac{\partial \tilde{w}_{\mathrm{a}}}{\partial \tilde{z}})_{\mathrm{ap}}\,, \qquad c_2 \equiv 2\pi(\frac{\partial \tilde{w}_{\mathrm{a}}}{\partial \tilde{z}})_O\,, \tag{D.7}$$

$$c_3 \equiv -\pi\int_0^{\tilde{z}_{\mathrm{ap}}} \frac{1}{\tilde{r}}\frac{\partial}{\partial \tilde{r}}(\tilde{r}\frac{\partial \tilde{w}_{\mathrm{a}}}{\partial \tilde{r}})\,\mathrm{d}\tilde{z} \quad \text{at } r = 0, \tag{D.8}$$

$$c_4 \equiv -\pi\int_0^1 \frac{\partial^2 \tilde{u}_{\mathrm{a}}}{\partial \tilde{z}^2}(\tilde{r}^2 - 1)\,\mathrm{d}\tilde{r} \quad \text{at } z = 0. \tag{D.9}$$

Our next task is to transform Eqs. (D.7)–(D.9) in terms of the stream functions in the domains A and B, which are parameterized by the respective curvilinear coordinates (Fig. 3). Because the stream function is an odd function of the radial coordinate, its series expansion close to the axis of symmetry reads [1]:

$$\psi_{\mathrm{f}} = (\frac{\partial \psi_{\mathrm{f}}}{\partial \tilde{r}})_{r=0}\tilde{r} + \frac{1}{3!}(\frac{\partial^3 \psi_{\mathrm{f}}}{\partial \tilde{r}^3})_{r=0}\tilde{r}^3 + \frac{1}{5!}(\frac{\partial^5 \psi_{\mathrm{f}}}{\partial \tilde{r}^5})_{r=0}\tilde{r}^5 + \ldots \quad (\mathrm{f} = \mathrm{a, b}). \tag{D.10}$$

From Eqs. (D10) and (3.7), we derive the respective series for the vertical velocity component:

$$\tilde{w}_{\mathrm{f}} = -2(\frac{\partial \psi_{\mathrm{f}}}{\partial \tilde{r}})_{r=0} - \frac{4}{3!}(\frac{\partial^3 \psi_{\mathrm{f}}}{\partial \tilde{r}^3})_{r=0} \tilde{r}^2 - \frac{6}{5!}(\frac{\partial^5 \psi_{\mathrm{f}}}{\partial \tilde{r}^5})_{r=0} \tilde{r}^4 + ... \text{ (f = a, b).} \qquad \text{(D.11)}$$

Therefore, c_1 and c_2 can be calculated using the following expression:

$$\frac{\partial \tilde{w}_{\mathrm{a}}}{\partial \tilde{z}} = -2\frac{\partial^2 \psi_{\mathrm{a}}}{\partial \tilde{r} \partial \tilde{z}} \text{ at } r = 0. \qquad \text{(D.12)}$$

From Eqs. (4.9), (4.10), and (D.12) written at the drop apex ($x_1 = 0$ and $x_2 = \alpha$), one obtains:

$$(\frac{\partial \tilde{w}_{\mathrm{a}}}{\partial \tilde{z}})_{\mathrm{ap}} = (1+\cos\alpha)[\sin\alpha \frac{\partial \psi_{\mathrm{a}}}{\partial x_1} - (1+\cos\alpha)\frac{\partial^2 \psi_{\mathrm{a}}}{\partial x_1 \partial x_2}]_{\mathrm{ap}} . \qquad \text{(D.13)}$$

With the help of Eqs. (4.4) and (4.8), the boundary condition (4.18) can be represented in the form:

$$\frac{1+x_1^2+(1-x_1^2)\cos\alpha}{(1-x_1^2)}\frac{\partial \psi_{\mathrm{a}}}{\partial x_2} + \psi_{\mathrm{a}} \sin\alpha = 0 \text{ at } x_2 = \alpha. \qquad \text{(D.14)}$$

The first derivative of Eq. (D.14) with respect to x_1, written at the drop apex, reads:

$$[(1+\cos\alpha)\frac{\partial^2 \psi_{\mathrm{a}}}{\partial x_1 \partial x_2} + \sin\alpha \frac{\partial \psi_{\mathrm{a}}}{\partial x_1}]_{\mathrm{ap}} = 0 . \qquad \text{(D.15)}$$

Using Eqs. (D.13) and (D.15), we calculate:

$$(\frac{\partial \tilde{w}_{\mathrm{a}}}{\partial \tilde{z}})_{\mathrm{ap}} = 2\sin\alpha(1+\cos\alpha)(\frac{\partial \psi_{\mathrm{a}}}{\partial x_1})_{\mathrm{ap}} . \qquad \text{(D.16)}$$

The first derivative of the boundary condition (4.17) with respect to x_1, written at the drop apex, gives:

$$(\frac{\partial \psi_{\mathrm{a}}}{\partial x_1})_{\mathrm{ap}} = -1 . \qquad \text{(D.17)}$$

Thus, we obtain the following exact analytical expression for c_1:

$$c_1 = -2\pi \sin\alpha(1+\cos\alpha) . \qquad \text{(D.18)}$$

Eqs. (C.4), (D.12) and (D.7) imply that c_2 could be calculated easier at the boundary of the domain A. Thus we obtain:

$$c_2 = -4\pi \frac{\partial^2 \psi_{\mathrm{a}}}{\partial x_1 \partial x_2} \text{ at } x_1 = 0 \text{ and } x_2 = 0\text{–}0. \qquad \text{(D.19)}$$

To calculate c_3, defined by Eq. (D.8), the values of the derivatives of the vertical velocity component at the axis of symmetry have to be obtained. From Eq. (D.11) it follows:

$$\tilde{r}\frac{\partial \tilde{w}_{\mathrm{f}}}{\partial \tilde{r}} = -\frac{8}{3!}(\frac{\partial^3 \psi_{\mathrm{f}}}{\partial \tilde{r}^3})_{r=0} \tilde{r}^2 - \frac{24}{5!}(\frac{\partial^5 \psi_{\mathrm{f}}}{\partial \tilde{r}^5})_{r=0} \tilde{r}^4 + ... \text{ (f = a, b)} \qquad \text{(D.20)}$$

and therefore,

$$\frac{1}{\tilde{r}}\frac{\partial}{\partial \tilde{r}}(\tilde{r}\frac{\partial \tilde{w}_{\mathrm{f}}}{\partial \tilde{r}}) = -\frac{8}{3}\frac{\partial^3 \psi_{\mathrm{f}}}{\partial \tilde{r}^3} \text{ at } r = 0 \text{ and f = a, b.} \tag{D.21}$$

In view of Eq. (D.21), the expression for c_3 reduces to:

$$c_3 = \frac{8\pi}{3}\int_0^{\tilde{z}_{\mathrm{ap}}} \frac{\partial^3 \psi_{\mathrm{a}}}{\partial \tilde{r}^3}\mathrm{d}\tilde{z} \text{ at } r = 0. \tag{D.22}$$

From the expression for the first derivative, Eq. (4.9), we deduce the following formula for the second derivative of the stream function with respect to the radial coordinate:

$$\frac{\partial^2 \psi_{\mathrm{f}}}{\partial r^2} = \frac{[(1-x_1^2)+(1+x_1^2)\cos x_2]^2}{4}\frac{\partial^2 \psi_{\mathrm{f}}}{\partial x_1^2} + \frac{x_1(\cos x_2 - 1)}{2}[(1-x_1^2)+(1+x_1^2)\cos x_2]\frac{\partial \psi_{\mathrm{f}}}{\partial x_1} +$$

$$+[(1-x_1^2)+(1+x_1^2)\cos x_2][\frac{2x_1 \sin x_2}{1-x_1^2}\frac{\partial^2 \psi_{\mathrm{f}}}{\partial x_1 \partial x_2} + \sin x_2 \frac{1+x_1^2}{(1-x_1^2)^2}\frac{\partial \psi_{\mathrm{f}}}{\partial x_2}] -$$

$$-\frac{x_1(1+x_1^2)\sin^2 x_2}{1-x_1^2}\frac{\partial \psi_{\mathrm{f}}}{\partial x_1} + \frac{4x_1^2 \sin^2 x_2}{(1-x_1^2)^2}\frac{\partial^2 \psi_{\mathrm{f}}}{\partial x_2^2} + \frac{4x_1^2 \sin x_2 \cos x_2}{(1-x_1^2)^2}\frac{\partial \psi_{\mathrm{f}}}{\partial x_2}. \tag{D.23}$$

Eqs. (4.9) and (D.23) imply that at the axis of symmetry (r = 0) we have:

$$\frac{8}{1+\cos x_2}\frac{\partial^3 \psi_{\mathrm{f}}}{\partial r^3} = (1+\cos x_2)^2 \frac{\partial^3 \psi_{\mathrm{f}}}{\partial x_1^3} + 12 \sin x_2 (1+\cos x_2)\frac{\partial^2 \psi_{\mathrm{f}}}{\partial x_1 \partial x_2} - 6\sin^2 x_2 \frac{\partial \psi_{\mathrm{f}}}{\partial x_1}. \tag{D.24}$$

From Eq. (4.6), we calculate the differential of the vertical coordinate in the domains B and C at the axis of symmetry:

$$\mathrm{d}\tilde{z} = \frac{\mathrm{d}x_2}{1+\cos x_2} \text{ at } x_1 = 0. \tag{D.25}$$

Finally, from Eqs. (D.22), (D.24), and (D.25) we derive the following expression for c_3:

$$c_3 = \frac{\pi}{3}\int_0^{\alpha}(1+\cos x_2)^2 \frac{\partial^3 \psi_{\mathrm{a}}}{\partial x_1^3}\mathrm{d}x_2 + 4\pi\int_0^{\alpha}\sin x_2 (1+\cos x_2)\frac{\partial^2 \psi_{\mathrm{a}}}{\partial x_1 \partial x_2}\mathrm{d}x_2 -$$

$$-2\pi\int_0^{\alpha}\sin^2 x_2 \frac{\partial \psi_{\mathrm{a}}}{\partial x_1}\mathrm{d}x_2 \text{ at } x_1 = 0. \tag{D.26}$$

Substituting the definition (3.7) into the integral in Eq. (D.9), one obtains:

$$c_4 = -\pi\int_0^1 \frac{\partial^3 \psi_{\mathrm{a}}}{\partial \tilde{z}^3}(\tilde{r}^2 - 1)\mathrm{d}\tilde{r} \text{ at z = 0.} \tag{D.27}$$

In view of Eq. (4.1), this integral is simpler in the domain A:

$$c_4 = \pi\int_0^1 \frac{\partial^3 \psi_{\mathrm{a}}}{\partial \tilde{z}^3}(1-x_1^2)\mathrm{d}x_1 \text{ at } z = 0\text{–}0 \text{ and } x_2 = 0\text{–}0. \tag{D.28}$$

Finally, using the formula for the third derivative in Eq. (C.4), we obtain:

$$c_4 = \pi \int_0^1 \left(\frac{\partial^3 \psi_a}{\partial x_2^3} + 6 \frac{\partial^2 \psi_a}{\partial x_2^2} + 6 \frac{\partial \psi_a}{\partial x_2} \right) (1 - x_1^2) \, \mathrm{d}x_1 \quad \text{at } x_2 = 0\text{–}0. \tag{D.29}$$

Appendix E. Expression for the force coefficient f_b

Integrating by parts in Eq. (5.9), we get:

$$f_b = \pi \int_1^\infty \tilde{p}_b \, \mathrm{d}(\tilde{r}^2 - 1) = -\pi \int_1^\infty (\tilde{r}^2 - 1) \frac{\partial \tilde{p}_b}{\partial \tilde{r}} \mathrm{d}\tilde{r} \quad \text{at } z = 0. \tag{E.1}$$

The derivative of pressure, which appears in the last integral, can be expressed from the Stokes equation (3.5), having in mind that the velocity at the membrane surface is zero:

$$f_b = -\pi \int_1^\infty (\tilde{r}^2 - 1) \frac{\partial^2 \tilde{u}_b}{\partial \tilde{z}^2} \mathrm{d}\tilde{r} \quad \text{at } z = 0. \tag{E.2}$$

With the help of the definition of the stream function, Eq. (3.7), we bring Eq. (E.2) in the form:

$$f_b = -\pi \int_1^\infty (\tilde{r}^2 - 1) \frac{\partial^3 \psi_b}{\partial \tilde{z}^3} \mathrm{d}\tilde{r} \quad \text{at } z = 0. \tag{E.3}$$

To calculate the last integral in terms of the curvilinear coordinates (Fig. 3), we apply the definitions (4.3) and (4.4) at the membrane surface:

$$\tilde{r} = \frac{1}{x_1}, \; \mathrm{d}\tilde{r} = -\frac{\mathrm{d}x_1}{x_1^2} \quad \text{at } x_2 = \pi. \tag{E.4}$$

From Eqs. (E.3) and (E.4), one obtains:

$$f_b = -\pi \int_0^1 \frac{1 - x_1^2}{x_1^4} \frac{\partial^3 \psi_b}{\partial \tilde{z}^3} \mathrm{d}x_1 \quad \text{at } z = 0. \tag{E.5}$$

To calculate the third derivative that appears in Eq. (E.5), we substitute Eq. (C.7) into Eq. (C.9) and estimate the result at $x_2 = \pi$:

$$\frac{\partial^3 \psi_b}{\partial \tilde{z}^3} = -\frac{8x_1^6}{(1 - x_1^2)^3} \frac{\partial^3 \psi_b}{\partial x_2^3} + \frac{12x_1^4}{(1 - x_1^2)^2} \frac{\partial^2 \psi_b}{\partial x_1 \partial x_2} + \frac{4x_1^4 (3 + x_1^2)}{(1 - x_1^2)^3} \frac{\partial \psi_b}{\partial x_2}. \tag{E.6}$$

From the boundary condition (4.16), it follows that the last two terms in the right-hand side of Eq. (E.6) are zero, and therefore Eq. (E.5) reduces to the following final expression for the force coefficient:

$$f_{\mathrm{b}} = 8\pi\int_0^1 \frac{x_1^2}{(1-x_1^2)^2}\frac{\partial^3\psi_{\mathrm{b}}}{\partial x_2^3}\mathrm{d}\,x_1 \quad \text{at } x_2 = \pi; \tag{E.7}$$

see Eq. (5.22).

Appendix F. Expression for the force coefficient f_{ab}

To calculate the pressure at the drop apex, we in the Stokes equation (3.6) we set $r = 0$, and integrate with respect to the vertical coordinate. The result reads:

$$(\tilde{p}_{\mathrm{b}} - \frac{\partial\tilde{w}_{\mathrm{b}}}{\partial\tilde{z}})_{\mathrm{ap}} = -\int_{\tilde{z}_{\mathrm{ap}}}^{\infty}\frac{1}{\tilde{r}}\frac{\partial}{\partial\tilde{r}}(\tilde{r}\frac{\partial\tilde{w}_{\mathrm{b}}}{\partial\tilde{r}})\mathrm{d}\,\tilde{z} \quad \text{at } r = 0. \tag{F.1}$$

We took into account the fact that the dynamic pressure and the velocity vanish at infinity. Substituting Eq. (F.1) into Eq. (5.20) we obtain:

$$f_{\mathrm{ab}} = -\pi(\frac{\partial\tilde{w}_{\mathrm{b}}}{\partial\tilde{z}})_{\mathrm{ap}} - \pi\int_{\tilde{z}_{\mathrm{ap}}}^{\infty}\frac{1}{\tilde{r}}\frac{\partial}{\partial\tilde{r}}(\tilde{r}\frac{\partial\tilde{w}_{\mathrm{b}}}{\partial\tilde{r}})\mathrm{d}\,\tilde{z} \quad \text{at } r = 0. \tag{F.2}$$

Using the definition (D.7) and introducing the new notation,

$$c_5 \equiv -\pi\int_{\tilde{z}_{\mathrm{ap}}}^{\infty}\frac{1}{\tilde{r}}\frac{\partial}{\partial\tilde{r}}(\tilde{r}\frac{\partial\tilde{w}_{\mathrm{b}}}{\partial\tilde{r}})\mathrm{d}\,\tilde{z} \quad \text{at } r = 0, \tag{F.3}$$

we present the force coefficient f_{ab} in the form:

$$f_{\mathrm{ab}} = c_5 - c_1\,. \tag{F.4}$$

With the help of Eqs. (D.21) and (F.3), we obtain:

$$c_5 = \frac{8\pi}{3}\int_{\tilde{z}_{\mathrm{ap}}}^{\infty}\frac{\partial^3\psi_{\mathrm{b}}}{\partial\tilde{r}^3}\mathrm{d}\,\tilde{z} \quad \text{at } r = 0. \tag{F.5}$$

In Eq. (F.5), $\tilde{z}_{\mathrm{ap}}$ corresponds to $x_2 = \alpha$ and the infinity point is given by $x_2 = \pi$. Then, combining Eqs. (D.24), (D.25), and (F.5), we derive the final expression for c_5:

$$c_5 = \frac{\pi}{3}\int_{\alpha}^{\pi}(1+\cos x_2)^2\frac{\partial^3\psi_{\mathrm{b}}}{\partial x_1^3}\mathrm{d}\,x_2 + 4\pi\int_{\alpha}^{\pi}\sin x_2(1+\cos x_2)\frac{\partial^2\psi_{\mathrm{b}}}{\partial x_1\partial x_2}\mathrm{d}\,x_2 -$$

$$-2\pi\int_{\alpha}^{\pi}\sin^2 x_2\frac{\partial\psi_{\mathrm{b}}}{\partial x_1}\mathrm{d}\,x_2 \quad \text{at } x_1 = 0; \tag{F.6}$$

see Eq. (5.27).

Appendix G. Solution of the hydrodynamic problem in the outer phase for α = 0

If the protrusion angle α is equal to zero, the hydrodynamic problem in the outer phase (described in Section 3) has an exact solution. Indeed, eliminating the velocity from the Stokes equations (3.4)–(3.6), we obtain a Laplace-type equation for the pressure:

$$\frac{1}{\tilde{r}}\frac{\partial}{\partial\tilde{r}}(\tilde{r}\frac{\partial\tilde{p}_{\rm b}}{\partial\tilde{r}})+\frac{\partial^2\tilde{p}_{\rm b}}{\partial\tilde{z}^2}=0\,. \qquad \text{(G.1)}$$

Using the Hankel transformation [3], and the fact that the pressure tends to zero at large distance z from the capillary, the general solution of Eq. (G.1) can be presented in the form:

$$\tilde{p}_{\rm b}(\tilde{r},\tilde{z})=\int_0^\infty A(k)J_0(k\tilde{r})\exp(-k\tilde{z})k\,{\rm d}\,k\,, \qquad \text{(G.2)}$$

where J_0 is the zero-order Bessel function and $A(k)$ is an unknown function, which is to be determined from the boundary conditions. Substituting the general solution (G.2) into the Stokes equation (3.6), and solving the resulting equation, we derive the following integral expression for the vertical velocity component:

$$\tilde{w}_{\rm b}(\tilde{r},\tilde{z})=\int_0^\infty [A(k)\frac{\tilde{z}}{2}+B(k)]J_0(k\tilde{r})\exp(-k\tilde{z})k\,{\rm d}\,k\,. \qquad \text{(G.3)}$$

Eq. (G.3) contains a new unknown function, $B(k)$, that could be found from the boundary conditions.

Because of the boundary conditions, the radial component of velocity, $u_{\rm b}$, is equal to zero at z = 0 for α = 0. Hence, from the continuity equation (3.4), written at z = 0, it follows that:

$$\frac{\partial\tilde{w}_{\rm b}}{\partial\tilde{z}}=0 \ \text{ at } z=0. \qquad \text{(G.4)}$$

From Eqs. (G.3) and (G.4), we obtain:

$$B(k)=\frac{A(k)}{2k} \qquad \text{(G.5)}$$

and

$$\tilde{w}_{\rm b}(\tilde{r},\tilde{z})=\frac{1}{2}\int_0^\infty A(k)(1+k\tilde{z})J_0(k\tilde{r})\exp(-k\tilde{z})\,{\rm d}\,k\,. \qquad \text{(G.6)}$$

The boundary condition, Eq. (2.12), reduces to the Poiseuille-flow expression, Eq. (2.2) for α = 0, which can be presented in terms of the dimensionless variables:

$$\tilde{w}_{\mathrm{b}} = 2(1-\tilde{r}^{2}) \text{ at } z = 0 \text{ and } 0 \le \tilde{r} \le 1. \tag{G.7}$$

From the integral representation (G.6), from the boundary condition at the membrane surface, and from Eq. (G.7) it follows that the unknown function $A(k)$ must satisfy the following conditions:

$$\int_{0}^{\infty} A(k) J_{0}(k\tilde{r})\, \mathrm{d}k = 4(1-\tilde{r}^{2}) \text{ at } 0 \le \tilde{r} \le 1, \tag{G.8}$$

$$\int_{0}^{\infty} A(k) J_{0}(k\tilde{r})\, \mathrm{d}k = 0 \text{ at } 1 \le \tilde{r}\,. \tag{G.9}$$

Taking the inverse Hankel transformation of Eqs. (G.8) and (G.9), we derive [4]:

$$A(k) = 4k\int_{0}^{1} J_{0}(k\tilde{r})(1-\tilde{r}^{2})\tilde{r}\, \mathrm{d}\tilde{r} = \frac{8}{k} J_{2}(k)\,, \tag{G.10}$$

where J_2 is the second order Bessel function.

From the definition (5.20), we obtain the force coefficient, f_{ab}, for $\alpha = 0$:

$$f_{\mathrm{ab}}(0) = \pi\, \tilde{p}_{\mathrm{b}}(0,0)\,. \tag{G.11}$$

Substituting Eqs. (G.2) and (G.10) into Eq. (G.11), one derives [4]:

$$f_{\mathrm{ab}}(0) = 8\pi\int_{0}^{\infty} J_{2}(k)\, \mathrm{d}k = 8\pi\,. \tag{G.12}$$

To determine the value of the force coefficient, f_{b}, we will use the definition (5.1), which yields:

$$f_{\mathrm{b}}(0) = -2\pi\int_{0}^{1} \tilde{p}_{\mathrm{b}}(\tilde{r},0)\tilde{r}\, \mathrm{d}\tilde{r}\,. \tag{G.13}$$

Combining Eqs. (G.2) and (G.10), we obtain an expression for the pressure at $z = 0$:

$$\tilde{p}_{\mathrm{b}}(\tilde{r},0) = 8\int_{0}^{\infty} J_{2}(k) J_{0}(k\tilde{r})\, \mathrm{d}k\,. \tag{G.14}$$

Substituting Eq. (G.14) into Eq. (G.13), we derive:

$$f_{\mathrm{b}}(0) = -16\pi\int_{0}^{\infty} J_{2}(k)\left[\int_{0}^{1} J_{0}(k\tilde{r})\tilde{r}\, \mathrm{d}\tilde{r}\right] \mathrm{d}k = -16\pi\int_{0}^{\infty} \frac{J_{1}(k)J_{2}(k)}{k}\, \mathrm{d}k\,, \tag{G.15}$$

where J_1 is the first order Bessel function; see Ref. [4]. The integral in the right hand side of Eq. (G.15) is of Weber-Schafheitlin type [4] and can be solved exactly. The result reads:

$$f_{\mathrm{b}}(0) = -\frac{32}{3}\,. \tag{G.16}$$

Appendix H. Application of the lubrication approximation in the wedge-shaped region of the outer phase for large protrusion angles

For $\alpha\to\pi$, the difference $\pi - \alpha$ can be used as a small parameter when solving the hydrodynamic problem in the outer phase. We will denote by v_1 and v_2 the components of the dimensionless velocity in the outer phase with respect to the curvilinear coordinate system. From the general assumptions of the lubrication approximation [5], it follows that: (i) The leading order function for the pressure depends only on the coordinate x_1:

$$\tilde{p}_{\mathrm{b}}(x_1, x_2) \approx \tilde{p}_{\mathrm{b}}(x_1)\,, \tag{H.1}$$

(ii) The velocity components obey the following general conditions:

$$v_1 >> v_2 \ \text{ and } \ \frac{\partial v_1}{\partial x_1} \approx \frac{\partial v_2}{\partial x_2}\,. \tag{H.2}$$

With the help of the vectorial identity [1]

$$\nabla^2 \mathbf{v}_{\mathrm{b}} = \nabla(\nabla\cdot\mathbf{v}_{\mathrm{b}}) - \nabla\times(\nabla\times\mathbf{v}_{\mathrm{b}}) \tag{H.3}$$

we represent the Stokes equations (3.1) in the form:

$$\eta_{\mathrm{b}}\nabla\times(\nabla\times\mathbf{v}_{\mathrm{b}}) = -\nabla p_{\mathrm{b}}\,, \tag{H.4}$$

where ∇ is the spatial gradient operator. In the case of rotational symmetry, the curl of velocity has only one component directed along the vector $\mathbf{e}_\phi$, where ϕ is the azimuthal angle. In our curvilinear coordinates, the dimensionless curl is [1]:

$$(\nabla\times\tilde{\mathbf{v}}_{\mathrm{b}})_\phi = \frac{1}{h_1 h_2}\left[\frac{\partial}{\partial x_1}(h_2 v_2) - \frac{\partial}{\partial x_2}(h_1 v_1)\right]. \tag{H.5}$$

In view of Eq. (H.5), the Stokes equation (H.4) acquires the following dimensionless form:

$$\frac{1}{h_2\tilde{r}}\frac{\partial}{\partial x_2}[\tilde{r}(\nabla\times\tilde{\mathbf{v}}_{\mathrm{b}})_\phi] = -\frac{1}{h_1}\frac{\partial\tilde{p}_{\mathrm{b}}}{\partial x_1}\,, \tag{H.6}$$

$$\frac{1}{h_1\tilde{r}}\frac{\partial}{\partial x_1}[\tilde{r}(\nabla\times\tilde{\mathbf{v}}_{\mathrm{b}})_\phi] = \frac{1}{h_2}\frac{\partial\tilde{p}_{\mathrm{b}}}{\partial x_2}\,. \tag{H.7}$$

Equation (H.7) confirms that in lubrication approximation, the pressure depends only on x_1 [5], in agreement with Eq. (H.1). Therefore, using Eqs. (4.3), (4.4), and (4.8), we obtain the lubrication approximation of Eq. (H.6):

$$\frac{\partial}{\partial x_2}[\tilde{r}(\nabla\times\tilde{\mathbf{v}}_{\mathrm{b}})_\phi] = -x_1(1-x_1^2)\frac{\mathrm{d}\tilde{p}_{\mathrm{b}}}{\mathrm{d}x_1}\frac{1}{h}\,. \tag{H.8}$$

Integrating Eq. (H.8) with respect to x_2, one derives:

$$\tilde{r}(\nabla\times\tilde{\mathbf{v}}_{\mathrm{b}})_{\phi}=-x_1(1-x_1^2)\frac{\mathrm{d}\,\tilde{p}_{\mathrm{b}}}{\mathrm{d}\,x_1}\Phi(x_1,x_2)-A_1(x_1)\,, \tag{H.9}$$

where $A_1(x_1)$ is an unknown function, which is to be determined from the boundary conditions; the function $\Phi(x_1,x_2)$ and $\varphi(x_1,x_2)$ are defined as follows:

$$\Phi(x_1,x_2)\equiv\frac{\varphi(x_1,x_2)}{x_1}\,;\qquad \varphi(x_1,x_2)\equiv\arctan[x_1\tan(\frac{x_2}{2})]\,. \tag{H.10}$$

In view of Eq. (H.2), equation (H.5) reduces to:

$$(\nabla\times\tilde{\mathbf{v}}_{\mathrm{b}})_{\phi}=-\frac{1}{h_1h_2}\frac{\partial}{\partial\,x_2}(h_1v_1)\,. \tag{H.11}$$

Substituting Eq. (H.11) into Eq. (H.9), and using Eqs. (4.3), (4.4), and (4.8), we obtain:

$$\frac{\partial}{\partial\,x_2}(h_1v_1)=(1-x_1^2)^2\frac{\mathrm{d}\,\tilde{p}_{\mathrm{b}}}{\mathrm{d}\,x_1}[\frac{\Phi(x_1,x_2)}{h}+\frac{A_1(x_1)}{h}]\,. \tag{H.12}$$

Integrating Eq. (H.12) with respect to x_2, one derives:

$$h_1v_1=(1-x_1^2)^2\frac{\mathrm{d}\,\tilde{p}_{\mathrm{b}}}{\mathrm{d}\,x_1}[\frac{\Phi^2(x_1,x_2)}{2}+A_1(x_1)\Phi(x_1,x_2)+A_2(x_1)]\,, \tag{H.13}$$

where $A_2(x_1)$ is an unknown function, which is to be determined from the boundary conditions. At both drop and membrane surfaces, which correspond to $x_2=\alpha$ and $x_2=\pi$, respectively, the velocity component v_1 is equal to zero. Appling these boundary conditions to Eq. (H.13), we get the final expression for the velocity component:

$$h_1v_1=\frac{(1-x_1^2)^2}{2}\frac{\mathrm{d}\,\tilde{p}_{\mathrm{b}}}{\mathrm{d}\,x_1}[\Phi(x_1,x_2)-\Phi(x_1,\alpha)][\Phi(x_1,x_2)-\Phi(x_1,\pi)]\,. \tag{H.14}$$

Note that the pressure distribution in Eq. (H.14) is unknown and it must be calculated, which is a usual procedure in the lubrication approximation [5]. For this goal, we use the continuity equation in curvilinear coordinates [5]:

$$\frac{\partial}{\partial\,x_1}(h_2\tilde{r}v_1)+\frac{\partial}{\partial\,x_2}(h_1\tilde{r}v_2)=0\,. \tag{H.15}$$

Equation (H.15) is integrated with respect to x_2 from α to π to obtain:

$$\frac{\mathrm{d}}{\mathrm{d}\,x_1}(\int_{\alpha}^{\pi}h_2\tilde{r}v_1dx_2)=h_1\tilde{r}v_2\big|_{x_2=\alpha}-h_1\tilde{r}v_2\big|_{x_2=\pi}\,. \tag{H.16}$$

The last term in the right-hand side of Eq. (H.16) is equal to zero because the velocity at the membrane surface is zero. The first term in the right-hand side of Eq. (H.16) is to be calculated from the boundary condition at the drop surface, Eq. (2.12). Thus, Eq. (H.16) reduces to:

$$\frac{\mathrm{d}}{\mathrm{d}\,x_1}(\int_\alpha^\pi h_2\tilde{r}v_1 dx_2) = \frac{4x_1(1-x_1^2)}{[1+x_1^2+(1-x_1^2)\cos\alpha]^3}(1+\cos\alpha)^2\,. \tag{H.17}$$

Integrating Eq. (H.17) from x_1 to $x_1 = 1$ (the edge of the pore), and taking into account that the velocity at the edge of the pore is zero, one obtains:

$$\int_\alpha^\pi h_2\tilde{r}v_1 dx_2 = -\frac{(1-x_1^2)^2(1+\cos\alpha)^2}{2[1+x_1^2+(1-x_1^2)\cos\alpha]^2}\,. \tag{H.18}$$

After some mathematical transformations, using Eqs. (H.14), (4.3), (4.4), and (4.8) one derives the following expression for the term in the left-hand side of Eq. (H.18):

$$\int_\alpha^\pi h_2\tilde{r}v_1 dx_2 = \frac{x_1(1-x_1^2)^3}{2}\frac{\mathrm{d}\,\tilde{p}_\mathrm{b}}{\mathrm{d}\,x_1}\int_\alpha^\pi [\Phi(x_1,x_2)-\Phi(x_1,\alpha)][\Phi(x_1,x_2)-\Phi(x_1,\pi)]\frac{\mathrm{d}\,x_2}{h}\,. \tag{H.19}$$

The integral in the right-hand side of Eq. (H.19) can be solved analytically:

$$\int_\alpha^\pi h_2\tilde{r}v_1 dx_2 = -\frac{(1-x_1^2)^3}{12x_1^2}\frac{\mathrm{d}\,\tilde{p}_\mathrm{b}}{\mathrm{d}\,x_1}[\frac{\pi}{2}-\varphi(x_1,\alpha)]^3\,, \tag{H.20}$$

where we have used also the definition of the function $\Phi(x_1,x_2)$, Eq. (H.10). From Eqs. (H.18) and (H.20), we derive the final analytical expression for the gradient of pressure:

$$\frac{(1-x_1^2)}{x_1^2}\frac{\mathrm{d}\,\tilde{p}_\mathrm{b}}{\mathrm{d}\,x_1} = 6(1+\cos\alpha)^2[1+x_1^2+(1-x_1^2)\cos\alpha]^{-2}[\frac{\pi}{2}-\varphi(x_1,\alpha)]^{-3}\,. \tag{H.21}$$

To obtain the contribution, f_wedge, of the hydrodynamic resistance in the wedge-shaped region between the drop and the horizontal solid wall (Fig. 1), we represent Eq. (E.1) in the form:

$$f_\mathrm{wedge} = \pi\int_0^1 \frac{1-x_1^2}{x_1^2}\frac{\mathrm{d}\,\tilde{p}_\mathrm{b}}{\mathrm{d}\,x_1}\mathrm{d}\,x_1\,. \tag{H.22}$$

Substituting Eq. (H.21) into Eq. (H.22), we derive the final expression for the respective force coefficient:

$$f_\mathrm{wedge} = 6\pi(1+\cos\alpha)^2\int_0^1 [1+x_1^2+(1-x_1^2)\cos\alpha]^{-2}\{\frac{\pi}{2}-\arctan[x_1\tan(\frac{\alpha}{2})]\}^{-3}\,\mathrm{d}\,x_1\,. \tag{H.23}$$

Introducing a new integration variable, $t \equiv \arctan[x_1\tan(\alpha/2)]$, the right-hand side of Eq. (H.23) can be simplified:

$$f_\mathrm{wedge} = 6\pi\cot(\frac{\alpha}{2})\int_0^{\alpha/2}\frac{8\cos^2 t}{(\pi-2t)^3}\mathrm{d}\,t\,. \tag{H.24}$$

The integral in Eq. (H.24) can be expressed as follows [4]:

$$\int_0^{\alpha/2} \frac{8\cos^2 t}{(\pi-2t)^3}\,\mathrm{d}t = \mathrm{ci}(\pi) - \mathrm{ci}(\pi-\alpha) + \frac{1-\cos(\pi-\alpha)}{(\pi-\alpha)^2} + \frac{\sin(\pi-\alpha)}{\pi-\alpha} - \frac{2}{\pi}\,, \tag{H.25}$$

where ci is the cosine integral [4] defined by the relationship:

$$\mathrm{ci}(x) \equiv -\int_x^{\infty} \frac{\cos t}{t}\,\mathrm{d}t\,. \tag{H.26}$$

In our case, $\pi - \alpha$ is a small parameter, and then Eq. (H.25) can be expanded in series:

$$\int_0^{\alpha/2} \frac{8\cos^2 t}{(\pi-2t)^3}\,\mathrm{d}t = 0.79381 - \ln(\pi-\alpha) + \frac{(\pi-\alpha)^2}{24} - \frac{(\pi-\alpha)^4}{1440} + \ldots\,. \tag{H.27}$$

Substituting Eq. (H.27) into Eq. (H.23), we obtain the final asymptotic expression for f_{wedge}:

$$f_{\mathrm{wedge}} = 6\pi\cot(\frac{\alpha}{2})[0.79381 - \ln(\pi-\alpha) + \frac{(\pi-\alpha)^2}{24} - \frac{(\pi-\alpha)^4}{1440}]\,; \tag{H.28}$$

see Eq. (5.31). We checked the precision of the asymptotic formula (H.28) and found that it gives the value of the integral (H.24) with a relative error smaller than 10^{-7} for $150° \leq \alpha \leq 180°$.

References

[1] G.A. Korn, T.M. Korn, Mathematical Handbook, McGraw–Hill, New York, 1968.

[2] G. Arfken, Mathematical Methods for Physicists, Academic Press, Orlando, FL, 1970.

[3] Yu.A. Brychkov, A.P. Prudnikov, Integral Transforms of Generalized Functions, Gordon and Breach, New York, 1989.

[4] M. Abramowitz, I.A. Stegun, Handbook of Mathematical Functions, National Bureau of Standards, Washington, DC, 1984.

[5] L.G. Leal, Laminar Flow and Convective Transport Processes: Scaling Principles and Asymptotic Analysis, Butterworth-Heinemann, MA, 1992.